ABSTRACT

McCOLGAN, GAIL EAGAN. Solution-processed Photodynamic Polymer Coating for Antimicrobial Surfaces. (Under the direction of Dr. Aram Amassian).

The prolonged survival of lethal pathogens on hard surfaces bears a major health risk to the global population. As demonstrated by the global COVID-19 pandemic, no one is safe from the treat of pathogens, especially airborne pathogens whose lifetime is extended 32x once deposited on a hard, non-porous surface. Exacerbated by the surge in hospitalizations due to COVID-19, the number of healthcare-associated infections increased since 2019. These infections can be caused by antibiotic resistant bacteria, necessitating inactivation before they are contracted, rather than treatment after. To prevent the spread of both SARS-CoV-2 and drug-resistant pathogens, antimicrobial materials are needed, those of particular interest being photodynamic materials. These materials use a photosensitizer, light, and oxygen to create reactive oxygen species, in order to inactivate pathogens through the oxidation of cellular components.

This thesis aims to expand on previous studies, which spray-coated *N*-methyl-4(4'-formyl-styryl)pyridinium methosulfate acetal poly(vinyl alcohol) a UV-crosslinkable polymer, containing various photosensitizers (zinc-tetra(4-*N*-methylpyridyl)porphine, methylene blue, and rose bengal) onto textile samples, which showed broad antimicrobial activity.

Analogous solutions were blade coated onto hard, non-porous substrates to provide precursory results of these photodynamic materials in non-textile applications. Optical microscopy, scanning electron microscopy, and ultraviolet-visible spectroscopy provided information on the surface morphology of the film and validated the coating's presence. Contact profilometry measured the dry film thickness for both the glass and nylon coated samples.

Antibacterial activity was studied using antimicrobial photodynamic inactivation assays against gram-positive methicillin-resistant *Staphylococcus aureus*. Inactivation ranging from 33.33-99.8% was achieved for photosensitizers tetra(4-*N*-methylpyridyl)porphine *p*-Toluenesulfonate, methylene blue, and rose bengal. The successful coating of photodynamic polymers onto solid substrates expands their use within hospital settings and extends it to public settings, providing increased protection from dangerous pathogens.

Solution-processed Photodynamic Polymer Coating for Antimicrobial Surfaces

by
Gail Eagan McColgan

A thesis submitted to the Graduate Faculty of
North Carolina State University
in partial fulfillment of the
requirements for the degree of
Master of Science

Materials Science & Engineering

Raleigh, North Carolina
2022

APPROVED BY:

Dr. Aram Amassian Committee Chair	Dr. Reza A. Ghiladi
Dr. Frank Scholle	

DEDICATION

To my parents, Marion and Michael McColgan, whose unyielding love and support has empowered me to not only work towards my goals, but grow into a kind, passionate, and tenacious woman.

To Brian Dulaney, Jayden Eppley, and Christian Boletchek, who always remind me that I am loved and never alone.

BIOGRAPHY

Gail Eagan McColgan was born in Cary, NC on February 22nd, 1999 to Marion and Michael McColgan. She began her college carrier studying Chemical Engineering with a minor in Materials Science at Northeastern University in Boston, MA. After careful consideration, Gail transferred to North Carolina State University in 2018, to both be closer to home and dive deeper into Materials Science. During her junior year of college, Gail decided that she wanted to continue her education by pursing a Master's degree and was accepted into the Advanced Bachelor's and Master's program at NC State. After doing an internship with a biopolymer start-up, Gail found a passion for biomaterials and medical textiles. Gail started doing research with the Amassian group on the fabrication of a prototype bioaerosol chamber for future use in antimicrobial materials research. After earning her bachelor's degree in May 2021, she began research on biocidal coatings. Following graduation, Gail hopes to continue working with biopolymers with aspirations in tissue engineering.

ACKNOWLEDGMENTS

I would like to thank my committee members, Dr. Aram Amassian, Dr. Reza A. Ghiladi, and Dr. Frank Scholle for their input and guidance on this project. Additionally, special thanks to Chuck Mooney for his assistance in taking SEM images and the bounds of life advice given within those 90 minutes.

I would like to thank those I hold most dear. First, my parents, Marion and Michael McColgan, for their constant love, encouragement, and willingness to talk through all of my challenges. Thank you to Brian Dulaney for always being my rock, even when 400 miles away. I am eternally grateful for the love and laughter that Jayden Eppley, my twin flame, has brought into my life. Lastly, even though work has moved us farther apart, Christian Boletchek has never failed to put a smile on my face when I needed it the most.

I would also like to acknowledge the researchers, and more importantly, friends, who have helped me through this degree. Thank you to Roland Ghareeb and Lihan Chen for helping me run aPDI assays and brainstorm about what caused the results. I would like to thank by fellow group members and others who I have collaborated with for the advice and laughter that they have given me, notably Zachary Campbell, Kasra Darabi, Boyu Guo, Ethan Strubinger, Laine Taussig, Tony Wang, and Nathan Woodward. I would like to give a special thank you to Tatiana Proksch for the endless conversation, memories, and help she has gifted me, and the invaluable editing she provided for my thesis.

The largest thank you that I could ever give, to Jake Mauthe, for everything that he has done for me over the last two years. From mentorship to casual conversation, research guidance to what I should eat for lunch, and all of the project-related humor, thank you. I will always remember *hospitals, wow*.

TABLE OF CONTENTS

LIST OF TABLES

LIST OF FIGURES

CHAPTER 1

Introduction

Respiratory diseases have been plaguing the world since there were humans inhabiting it. These diseases got exponentially worse after people settled into communities, rather than roaming the earth. Seasonal influenza contributes approximately ~250,000-650,000 deaths a year despite vaccines.[1] The COVID-19 pandemic has shown the devastating impact that an airborne virus can have on the globe. To date, worldwide there have been 458.5 million confirmed cases and 6 million deaths. The SARS-CoV-2 virus has significantly impacted the Americas, a region that ranks 2nd in cumulative cases (~33%) and 1st in cumulative deaths (~44%).[2]

The Centers for Disease Control and Prevention (CDC) suggests that the general public practice good hygiene, wear personal protective equipment (PPE), use disinfectants, and social distance. Face masks are primarily used to reduce the spread of infectious respiratory droplets and aerosols. One concerning issue is the re-aerosolization of settled particles from the mask. These particles may be agitated by coughing or sneezing and resettle on a hard surface leading to further contamination.[1,3] Hard non-porous surfaces increase pathogen lifetime and therefore transmission. The lifetime of SAR-CoV-2 has been shown to increase hours in the air to upwards of 4 days on dry surfaces or longer in warm, humid environments.[1,4]

In addition to the obvious effects of the SARS-CoV-2 virus, the pandemic has escalated an already prevalent concern within the United States healthcare system: nosocomial/healthcare-associated infections (HAIs). In 2002, approximately 1.7 million HAIs were estimated in the United States alone, with a ~5.8% mortality rate.[3,5] Approximately 20-40% of HAIs are transmitted by the hands of health care workers through contact with contaminated surfaces.[3,6] The implementation of preventative cleaning measures decreased the number of HAIs to roughly

722,000 in 2011.[6] However, in 2020 due to COVID-19, hospitalizations increased, leading to a sharp rise again in nosocomial contaminations.[7] One of the category of HAIs that increased above 33.8% in the fourth quarter of 2020 was methicillin-resistant *Staphylococcus aureus* (MRSA),[7] an antibiotic-resistant gram-positive bacteria that can live on hard surfaces for upwards of 7 months.[4,8]

The need for continuously disinfecting surfaces has become ever apparent throughout the COVID-19 pandemic, and from the inability to treat the rising number of HAIs with antibiotics.[9,10] Development of antimicrobial materials has increased. Of particular interest are antimicrobial (not containing drugs) polymer coatings and antimicrobial photodynamic inactivation (aPDI).[11]

The purpose of this thesis work is to investigate photodynamic inactivation and develop an antimicrobial polymer coating for hard non-porous surfaces. Previous work has been done using a UV-photocrosslinkable polymer: *N*-methyl-4(4'-formyl-styryl)pyridinium methosulfate acetal poly(vinyl alcohol) (SbQ-PVA), and various photosensitizers (zinc-tetra(4-*N*-methylpyridyl)porphine,[12] methylene blue, and rose bengal) on variety of textile substrates.[13] These photosensitizer/SbQ-PVA coated textiles exhibited antimicrobial efficacy against gram-negative and gram-positive bacteria and both enveloped and non-enveloped viruses.[12,13] The same polymer solution was coated on two hard, non-porous substrates and antibacterial activity against S. aureus was observed. This work is also designed as a control study to investigate solution processing without the challenges added from porous substrates, however, the results may provide insight into the use of porous materials. This contribution to the knowledge base of photodynamic material coatings will help infer the ability of these materials to be used on

common high-touch surfaces, such as hospital overbed tables, IV pump controls, and medical supply carts.[14]

CHAPTER 2

Organic Antimicrobial Materials

2.1 Antimicrobial Polymer Coatings

To create drug-free antimicrobial surfaces polymer-based coatings are optimal because they are durable, flexible, and inexpensive. By combining with disinfectants, they increase the lifetime and performance of antibacterial surfaces and decrease the frequency of manual cleaning.

Antimicrobial polymers can be classified by their antimicrobial activity and their polymer material type.[15,16] The mechanism of antimicrobial activity can be either passive or active.[15] Passive antimicrobial polymers do not actively kill bacteria. Instead, they deter bacterial adhesion through the reduction of protein adsorption on the contact surface via hydrophilic repulsion, electrostatic repulsion, or low surface energy[15,17]Active polymers are used for bacteria that adhere to the polymer surface. Active polymers are classified into three different polymeric material classes based on the biocidal agent used: biocidal polymers, polymeric biocides, or biocide-releasing polymers.[15,16] Biocidal polymers have antimicrobial sites located throughout the substance and the biocidal capacities are intrinsic in the material. Alternatively, polymeric biocides are created by covalently bonding biocidal molecules to the polymer back bone or chemically modify an existing function group to create a biocidal functional group.[15,16,18,19] The polymers that will be discussed in this research are biocide-releasing polymers. Biocide-releasing polymers are loaded with biocide molecules rather than covalently bonding them to the polymer. On mechanism of release is the cleavage of linkages between the polymer carrier and biocides, to release the biocide into the surrounding environmentenvironment.[15,16,19] Typical release particles

include metal nanoparticles, such as silver, copper, zinc oxide, and titanium dioxide nanoparticles, and antibiotics, such as vancomycin, ciprofloxacin, and levofloxacin.[18,19]

A new area of antimicrobial polymer research employs photodynamic inactivation (PDI) to kill pathogens. Photosensitizers (PS), are excited using light to react with ambient oxygen to create reactive oxygen species (ROS), which can inactivate a wide array of pathogens.[18,19] Photosensitizers in antimicrobial polymers can be considered both a biocide-releasing polymer material type or a polymeric biocide depending on how the photosensitizers are linked to the polymer.[16,18,19] New photosensitizer-containing polymer systems that have been synthesized using cellulose-based materials, not limited to: paper,[20-22] nanofibrillated cellulose,[23] and cellulose nanocrystals.[24,25] Photosensitizers have been added to nylon,[26] polyacrylonitrile,[26,27] and polystyrene[22] melts and electrospun to bond the PS to the ejected fibers. Textiles such as cotton[28] and wool blends[29] have been traditionally dyed with photosensitizers, where electrostatic attraction incorporates the PS into the polymer. Photosensitizers have been immobilized on a host of additional polymers, including polyurethan,[22,30] silicone,[22,31] chitosan,[22] polydimethylsiloxane,[22] and cellulose acetate.[22,32,33]

2.2 Photodynamic Inactivation

Photodynamic inactivation originated from the discovery of photodynamic therapy (PDT) in 1900 by Oskar Raam and Hermann von Trappeiner when a species of protozoans was killed after being stained with acridine orange and illumination.[34,] This led to the use of PDT as a cancer therapy in the 1970s and has continued to develop into therapies for localized infections and macular degeneration.[34] PDT uses a photosensitizer, or a material that easily absorbs photons, in conjunction with oxygen and visible light to produce ROS.[19,34,36-38] Photosensitizers can be

photoactive non-toxic dyes, which are typically aromatic chromophores with highly conjugated systems. The delocalized elections in the conjugated structure boost the vibrant color of the PS and lower the energy required for electron excitation.[34,38] Photosensitizers can also be fullerenes,[36,37,43,46,49] metal nanoparticles,[11,39,46,48,49,51,52] or quantum dots[48,53].

2.2.1 Mechanism of Reactive Oxygen Species Generation

The three components of PDT (PS, oxygen, light) are harmless individually, however, when combined and activated with light, bacteria-killing ROS are formed. The wavelength of the light must match the absorbance spectra of the PS.[19,34-43] Photosensitizers that are photoactive non-toxic dyes, are comprised of conjugated double bonds, allowing for delocalized π-electrons to be more easily excited from the highest occupied molecular orbital (HOMO) to the lowest unoccupied molecular orbital (LUMO). When there are enough conjugated double bonds, the energy needed to excite the electrons can be provided by visible light.[34,38]

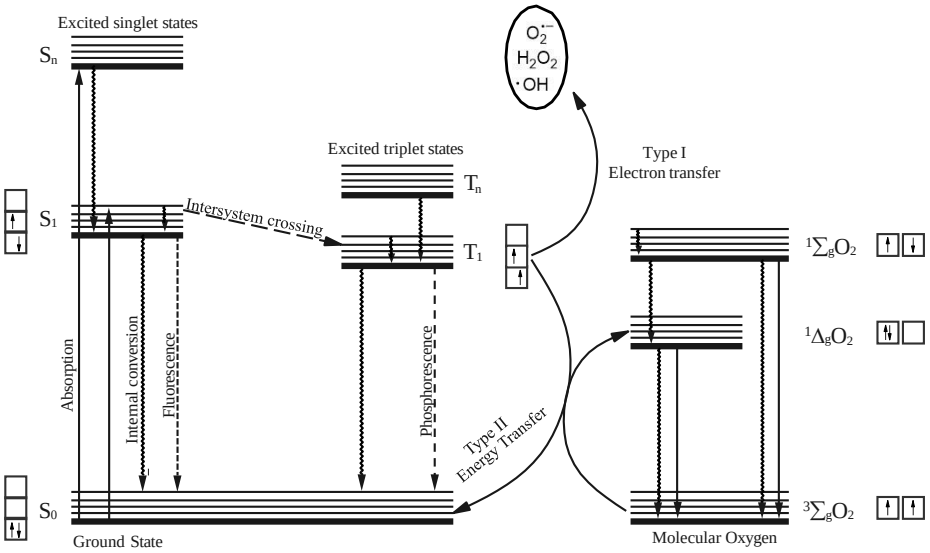

Figure 2.1 Jablonski energy diagram for the generation of reactive oxygen species (adapted from references 38 and 39)

When a ground-level singlet state of PS is illuminated with light representative of its absorbance peak an electron is excited from the HOMO to the LUMO. This electron creates a short-lived (nanoseconds) excited singlet state. Once in this excited singlet state, a non-radiative relaxation intersystem crossing can occur, which moves the PS to an excited triplet state that has less energy than the excited singlet state but a longer lifetime (microseconds). The triplet state PS can now interact with the surrounding molecular oxygen (Figure 2.1).[22,34,35-37,39-41,43]

One interaction between the PS in its triplet state and oxygen is a Type I interaction, where an electron is transferred from the PS to the oxygen to create a superoxide anion ($O_2^{\bullet -}$). This anion can form other reactive oxygen species such as hydroxyl radical (•OH) and hydrogen peroxide (H_2O_2). These ROS have a variety of different reactivities and biological defense mechanisms to deactivate them, include enzymatic reactions and antioxidant quenching.[22,34-39,41,42]

The second photochemical interaction is a Type II reaction. This reaction occurs when energy is transferred from the excited triplet state PS to molecular oxygen, causing the outermost electron (in the oxygen molecule) to reverse its spin and move into the orbital of an electron spinning in the same direction. The result is a short-lived and instable molecule termed singlet oxygen ($^1O_2$), which has a diffusion limit of ~1 mm in air and ~250 nm in aqueous conditions.[44] Type II-produced reactive oxygen species react differently than those produced by a Type I reaction. Single oxygen reacts with sites that have a high electron density such as sulfur groups and π-bonds. Cells are less-able to hinder singlet oxygen inactivation than compared to other radicals because singlet oxygen cannot be broken down through enzymatic reactions.[22,34-39,41-43]

2.2.2 Gram-positive Bacterial Inactivation

Reactive oxygen species impart most of their damage to the bacterial cell wall.[35,37,45,46] Photosensitizers are attracted to bacteria via an initial and expeditious electrostatic attraction. Gram-positive bacteria have a cell wall containing a peptidoglycan layer composed of proteins and lipetechoic acid which provide a negative charge. The negative surface charge on the bacterial cell wall preferentially binds to positively charged surfaces.[35,37,45,46] At the cell wall singlet oxygen oxidizes surface proteins to permeabilize the wall and cause it to start leaking. The weakening of the cell wall leads to the bacterial death. Oxidative stress is also imparted on enzymes, nucleic acid, and the cell membrane which cause irreversible damage, and ultimately destruction of bacteria (Figure 2.2).[46,47] The inactivation of the gram-positive bacterium MRSA was employed in this research for initial results on bacterial inactivation and its ties to the work's motivation.

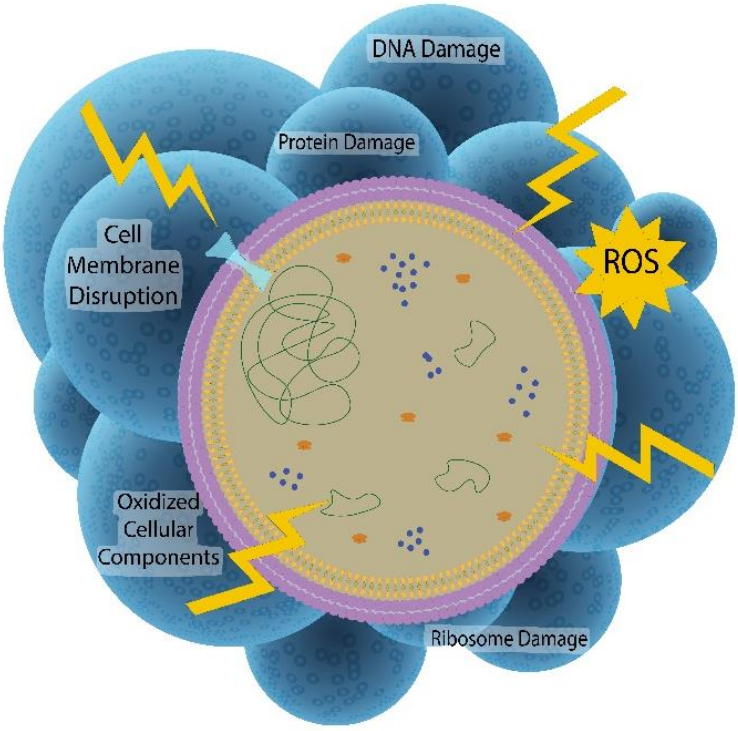

Figure 2.2 Inactivation of bacteria by reactive oxygen species (adapted from reference 47)

2.2.3 Photosensitizers

Photosensitizers must be able to effectively absorb specific wavelengths of visible light, have the appropriate energy while in their triplet state to transfer energy or electrons to create ROS, the complimentary quantum yield appropriate for the ROS desired, and high photostability.[34,36,40,41] Common photosensitizers types are listed in Table 2.1. Most PS have a system of heterocyclic rings to provide an abundance of delocalized electrons for excitation. Photosensitizers for therapeutic applications are the wide class of porphyrins which are highly researched since they have a fast intersystem crossing and a long lifetime when in their excited triplet state.[38,39] These molecules have high singlet oxygen quantum yield but are also expensive.[39] Phenothiazine dyes are also researched as antimicrobial photosensitizers. Methylene blue is commonly used due to its relatively low cost, commercial availability, and regulatory approval, however its photoactivity is lower than many other photosensitizers.[36] Natural derivatives such as Hypericin,[36,37,48] Hyopcreliin,[48] curcumin,[36,47] Purpin-18,[48] and Purpurinimide[48] are used for their green properties. Xanthene dyes, such as rose bengal, are frequently used as biological stains and diagnostic treatments.[49] The anionic nature of rose bengal hinders its antimicrobial efficacy as this repels similarly charged bacteria.[49]

Table 2.1 Photosensitizers

Photosensitizer	Examples
Anthraquinone derivatives	Hypericin,[36,37,48] Hypocrellin[48]
Cyanine dyes	Indocyanine green,[50] merocyanine,[50] pentamethine cyanine,[50] squaraine,[50]
Metal nanoparticles (NPs), quantum dots, fullerenes	Gold NPs,[46,48] Titanium dioxide NPs,[11,39,46,49,51], Zinc oxygen NPs,[11,51,52] Carbon nitride quantum dots,[48] manganese-doped zinc sulfide quantum dots,[53] fullerenes[36,37,43,46,49]
Natural derivatives (misc.)	Curcumin[36,47]
Phenothiazine dyes	Methylene blue,[0,35-37,40,4149] toluidine blue[36,37,40,41]
Phthalocyanine dyes	Aluminum disulphonated phthalocyanine,[39,40] cationic Zinc(II)-phthalocyanine,[39,40] naphthalocyanine[40]
Porphyrins	Bacteriochlorins,[36,38,39,40,48,49] Radachlorin,[41] sulfonated porphyrins,[48] Purpin-18,[48] Purpurinimide,[48] *meso*-tetra (*N*-methyl-4-pyridyl) porphine tetra tosylate,[34] tetraphenyl porphyrin,[48] Photofrin[40,41,49]
Xanthene dyes	Erythrosine,[40,41] rose bengal[37,41,49]

CHAPTER 3

Polymer Solution Processing

The essential components for solid-state materials prepared via solution-processing are dissolved and/or suspended solids in a liquid phase. The solvent evaporates to leave behind the solid polymer coating. Both solvent selection and composition can affect the rheology of the solution, which is important for both the coating process and cost. For coating, liquids need to wet and flow across the substrate, which requires low viscosity (~1-1000 mPa•s) and a low contact angle (high wettability).[54] However, this has both cost and drying time implications depending on the chosen materials. Choosing the most compatible volatile fluid is vital as it impacts the drying time and the miscibility of the solution. The use of expensive solvents for dissolution can dramatically increase costs.[54]

3.1 Solvent Quality and Solution Thermodynamics

Thermodynamic principles can be used to predict a solvent's ability to dissolve a polymer. The change in Gibbs free energy upon mixing (ΔGm) is always negative (Equation 1). Change in entropy (ΔSm) is positive as entropy increases with mixing. Change in enthalpy (ΔHm), or the heat of mixing, can be negative or positive and determines solubility.[54] The Flory-Huggins theory incorporates the statistical distribution of solvent and polymer molecules. The average radius of the polymer in respect to its center of mass (R), the moles (n_s, n_p), and volume fractions (ϕ_s, ϕ_p) of solvent and polymer are used to predict the entropy change during mixing (Equation 2). [54-56] Change in enthalpy from mixing (ΔH_m) can then be found (Equation 3). ΔH_m is dependent on the number of contact points between the polymer and solvent, and the solvent-solvent, polymer-polymer, and solvent-polymer interaction energies. The Flory-Huggins

parameter (χ) incorporates the interaction energies of the solvent-polymer system. The Gibbs free energy upon mixing (ΔG_m) can be expressed in terms of the solvent-polymer interactions (Equation 4). To obtain the necessary negative Gibbs free energy, a smaller χ value is favored.[54-56]

$$\Delta G_m = \Delta H_m - T\Delta S_m \quad (1)$$

$$\Delta S_m = -R\left[n_p \ln \phi_p + n_s \ln \phi_s\right] \quad (2)$$

$$\Delta H_m = n_s \phi_p \chi RT \quad (3)$$

$$\Delta G_m = RT\left[n_s \ln \phi_s + n_p \ln \phi_p + n_s \phi_p \chi\right] \quad (4)$$

The solubility parameter (δ) is based on the principle that materials dissolve in solvents with similar chemical compositions. It relates the heat of vaporization and molar volume, as a measure of the solution's cohesive energy density. The enthalpy of mixing changes with the square of the difference in solubility parameters of the solvent (δ_s) and the polymer (δ_p) (Equation 5). Therefore, a solvent should have a similar solubility parameter to that of the polymer for favorable dissolution.[54]

$$\Delta H_m \approx \phi_s \phi_p (\delta_s - \delta_p)^2 \quad (5)$$

The polymer molecular weight also influences solubility. Larger molecules, such as long-chain polymers, are harder to dissolve than small molecules, such as monomers. This study was primarily done using one polymer at a fixed molecular weight; therefore, the influence of molecular weight will not be discussed.

3.2 Rheology

The polymer solution rheology impacts the coating procedure and cost. The flow rate of a fluid dictates the coating speeds that can be used, the substrate dimensions, and the coating tool/dye. Increasing the concentration, *C*, of polymer in the solution will cause the polymer chains to overlap up to a max concentration *C**. The polymer-polymer interactions decrease the polymer chains' ability to move in the solution. Furthermore, when the polymer chains' overlap, they can become entangled and further hinder movement, significantly increasing viscosity of the solution (Figure 3.1). Concentrated solutions have an increased number of polymer-solvent interactions, increasing their folding, overlap, and eventual entanglement. However, if solutions are dilute, the solutions behave more like the solvent. At low concentrations polymer chains disentangle and elongate, allowing for chain motion and lowering solution viscosity.[54]

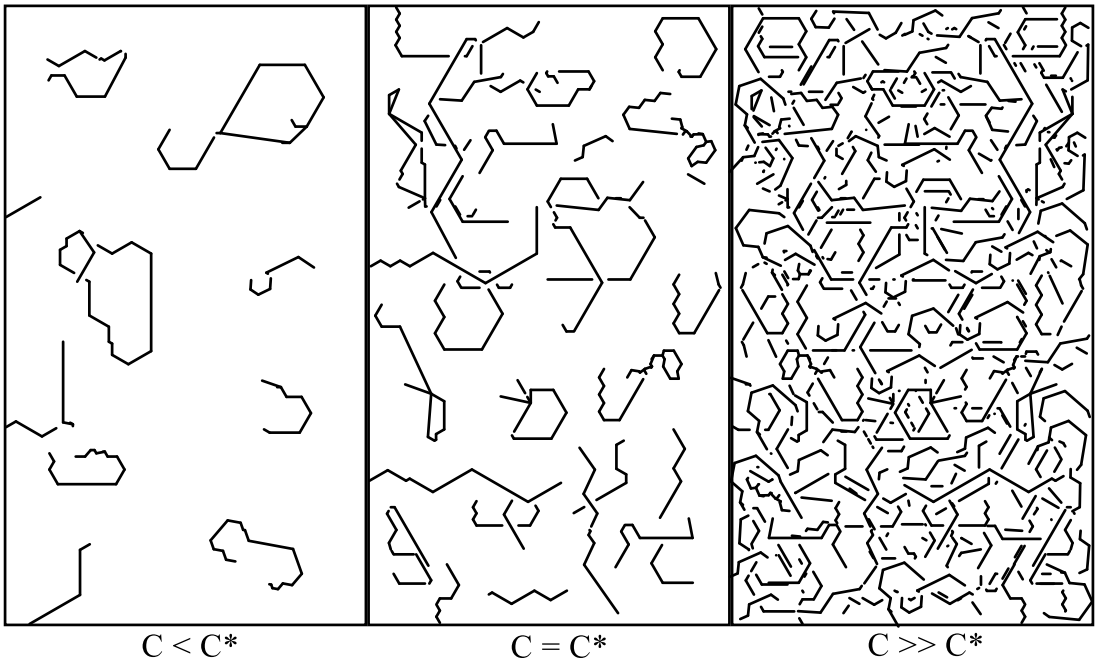

Figure 3.1 Polymer interaction and entanglement with increase concentration in solution (adapted from reference 54)

3.3 Drying

The rate of drying can dictate the microstructure and crystallinity of the solid.[54] The polymers used in this research are completely amorphous, so crystallization will not be discussed.

To obtain a dry polymer film the solvent must be evaporated from the wet film. The main concerns regarding drying of polymer solutions are long drying times and defects caused by confined shrinking. There are three steps to evaporative drying processes that occur in a series (Figure 3.2). The first step is the movement of solvent from the bulk to the free surface of the coating. This process is instantaneous as there is already solvent at the surface. Within the bulk of the material, solvent transport is dependent on the transport processes of the polymer solution used. The polymer-solvent system chosen should allow for adequate solvent diffusion throughout the solution. Second, the solvent at the surface evaporates and is, third, transported away from the coating and into the surrounding environment. The last two steps are external and dependent on the environmental conditions and the transport processes of the surrounding vapor pressures.[54]

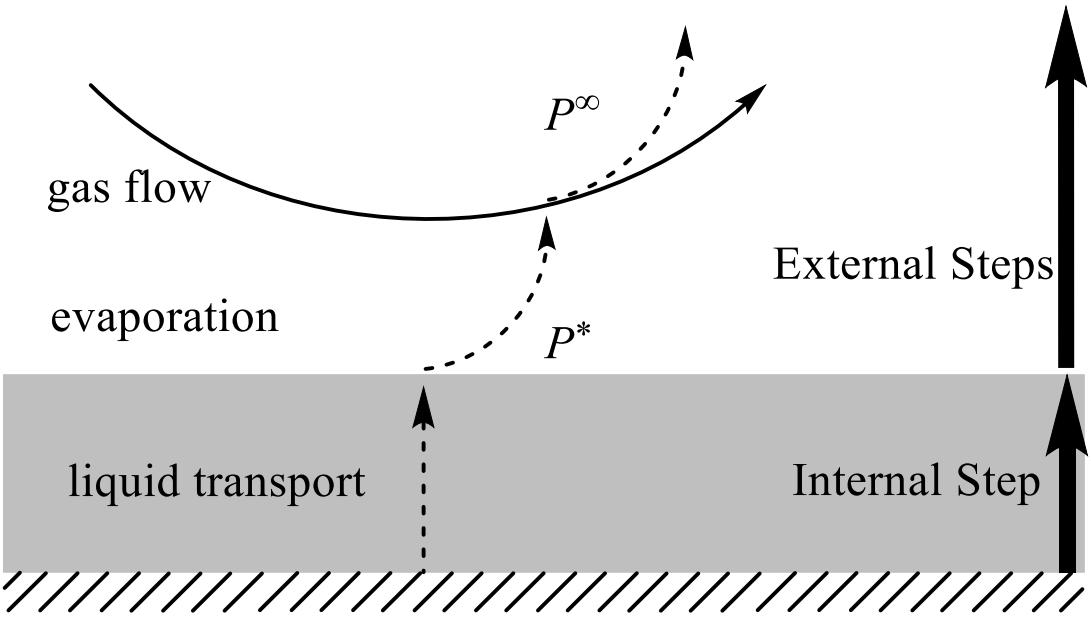

Figure 3.2 Diagram of drying steps for a polymer film (adapted from reference 54)

At the start of the drying process, the externally controlled steps are considered the rate-limiting steps. This is because the solvent is concentrated at or near the surface of the coating. Evaporation and gas transport is dependent on the partial pressure at the surface and in the surrounding gas. The liquid-vapor equilibrium dictates the partial pressure of the vapor at the free surface (P^*) and the surrounding gas dictates the partial pressure of the vapor a good distance from the surface (P^{∞}). For evaporation to occur the difference between these two partial pressures must be greater than zero. This can be aided by raising the temperature, thus raising P^*, or keeping the vapor concentration of the surrounding environment low, thus keeping P^{∞} low. While the solvent is continuously evaporated, the limiting factor changes from externally dictated steps to the internally dictated step involving solvent transport through the coating.[54]. The solvent has to pass through an increasingly concentrated amount of polymer to reach the free surface.[54,57] Each stage in the solvent evaporation process can be measured by weighing the loss

of material in the film (Figure 3.3). The rate is constant at the beginning of the drying process as the difference in partial pressures is fairly constant with a constant temperature. Once the drying rate begins to fall solvent transport controls the evaporation rate, which continues to decrease with increasing thickness of the dry film, until all the solvent is gone.[54]

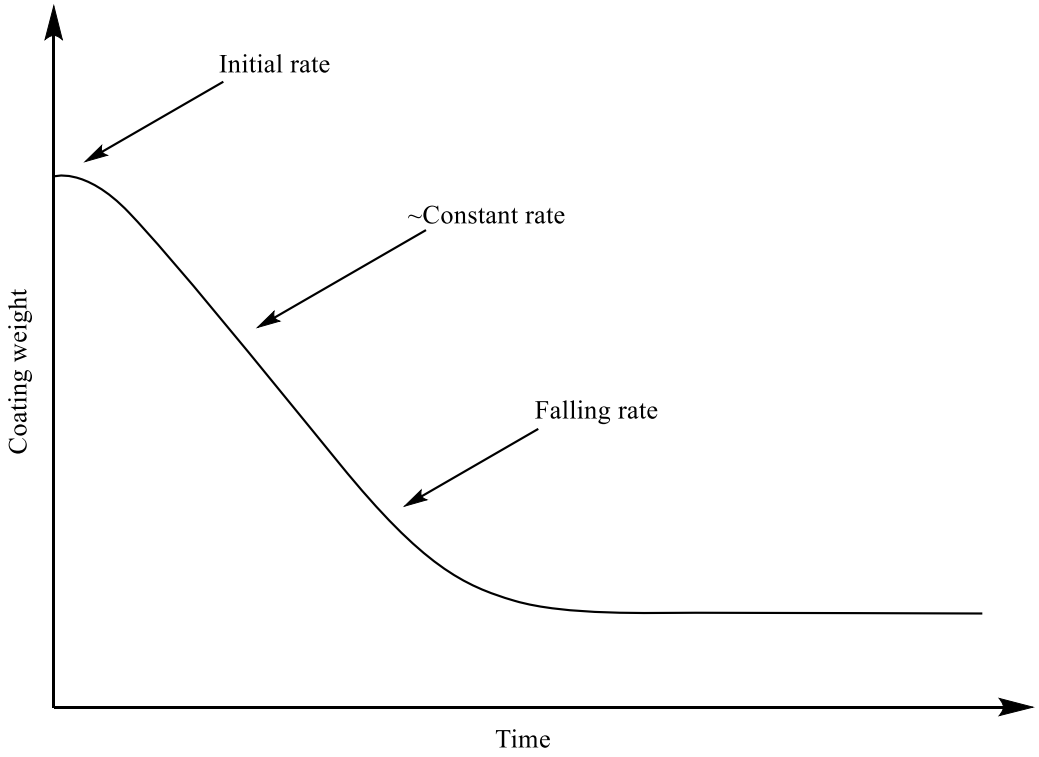

Figure 3.3 Weight loss from a polymer film, with rate dependence on the drying steps (adapted from reference 54)

3.4 Coating Techniques

There are a variety of coating techniques that are utilized for solution processing. These techniques include meniscus-based methods, such as dip, blade, wire bar, and slot-die coating, as well as spin-coating and spray-coating (Figure 3.4).[58]

Spin-coating uses a rotating substrate to distribute the dispensed solution evenly. The substrate is first spun at a low rpm, allowing the solution to spread from the center of the substrate to the edges. A faster rotation rate is then used to spin excess solution off the edges of the substrate and thin the solution out into a level coating. Evaporation of the solvent to continues the thinning process.[58,59]

Spray-coating involves spraying particles or liquids onto a substrate with subsequent drying. This is also seen as scalable ultrasonic spray coating, done at the picoliter scale with improved control and uniform coverage from both an inert coating environment and the high frequency of vibration used.[58,60]

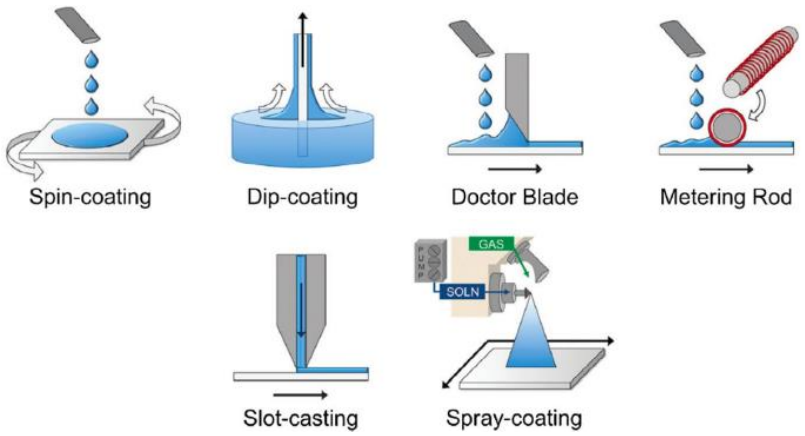

Figure 3.4 Solution processing methods (reference 60)

3.4.1 Meniscus-guided coating techniques

Meniscus-guided coating processes are defined by a dynamic meniscus that is guided across the substrate to create the film. The geometry of the meniscus allows for the wet film thickness to be calculated knowing the solution viscosity.[61,62] At lower coating speeds evaporation occurs at the surface of the meniscus, leaving behind an immediately dried film. The

thickness of the coating is dependent on the solvent evaporation at the meniscus, giving rise to the name “evaporation” regime. When in the evaporation regime decreasing the velocity requires increasing the blade height due to a higher polymer deposition rate.[54,59,64-67] At high speeds, the solution is deposited by viscous forces. As frictional drag increases a wet film is left behind which then dries. This is termed the Landau-Levich regime, named after the Landau-Levich equation which predicts the wet film thickness of a vertically drawn plate from a liquid. Within this regime continuously increasing the velocity, and thus the frictional drag, creates thicker coatings.[54,59,61,62,64-68] An example of these two regimes and their resultant film thickness can be seen in Figure 3.5 below for the coating of phospholipid films.

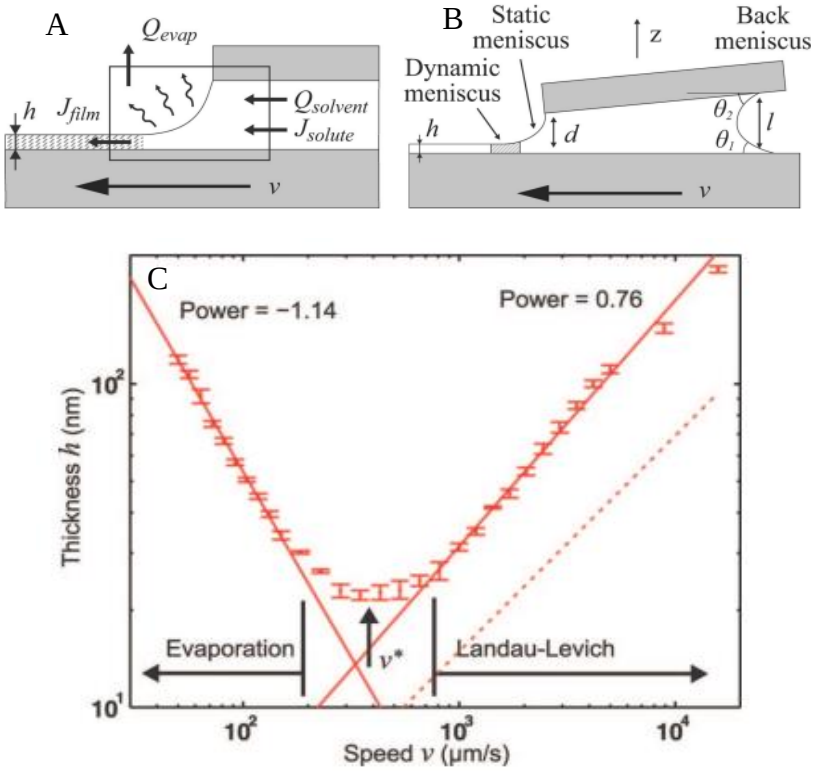

Figure 3.5 Diagram of (A) evaporation and (B) Landau-Levich regimes and (C) a plot of the change in film thickness with blade coating velocity (reference 66)

Dip-coating is the submersion of a substrate vertically into the coating solution and subsequently removing it at a constant rate with the solution adhered to the surface. The wet film thickness is proportional to the substrate speed and solution viscosity, while also taking into account the effect of gravity on the coating.[54,58-62] Blade coating moves a fixed rod, tightly wrapped in a thin wire, across a substrate to spread the solution. The rod height above the substrate is set, then the solution is dispensed at the base of the rod before motion.[58] Slot-die coating uses a coating head, or die, to dispense the solution onto the substrate at a specified rate. The substrate is moved beneath the die for coating. Slot-die coating is a scalable technique which often turns to blade coating for preliminary research efforts as there are fewer coating parameters to manipulate, then transitions to industrial scale slot-die instruments.[54,58,59]

Blade coating, also called doctor blade, knife, or flow coating, coats a substrate by spreading a solution with a stationary blade. The blade is fixed at a specified angle and gap height from the substrate and solution is dispensed between the blade and substrate. Once the meniscus is formed the blade is accelerated to a fixed velocity to allow for spreading (Figure 3.6). The solution is held between the blade and substrate by capillary forces while a small amount of the solution remains on the substrate as the blade travels past due to frictional drag.[54,58,59,64-69,70]

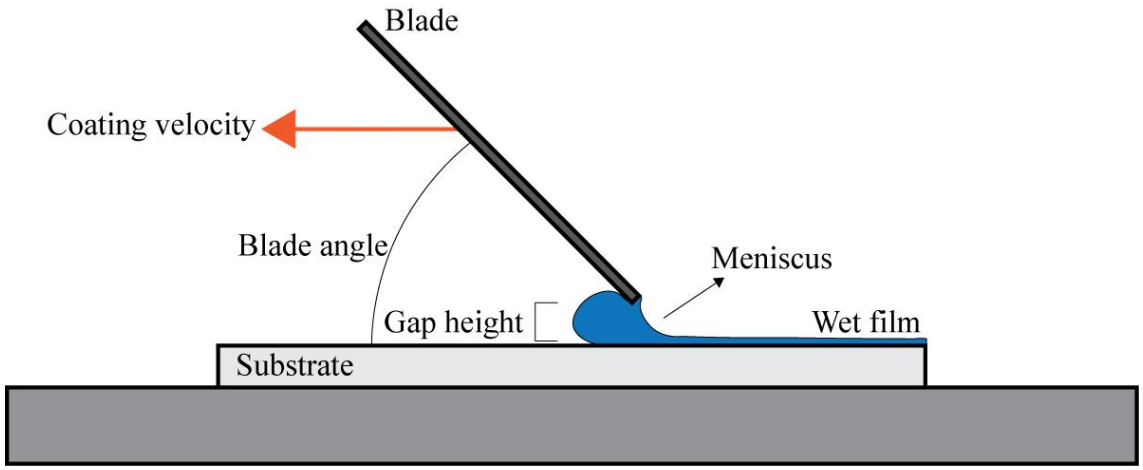

Figure 3.6 Blade coating schematic

The blade angle, gap height, coating velocity, solution concentration, and dispensed volume all contribute to the final film thickness. Higher blade angles, solution concentrations, and solution volume all increase the thickness of the coating.[70] Increasing the solution viscosity and volume both increase the amount of polymer available to be deposited and the frictional forces between the meniscus and the substrate.[67-70] Increasing the solution volume also increases the meniscus height, which experimentally shows to increase the coating thickness.[65,67,68,70] Conversely, increasing the gap height between the blade and the substrate decreases the coating thickness. This is due to the increase in meniscus height when compared to similar solution volumes at lower gap heights.[65,68,70] In regards to coating velocity, the evaporation and Landau-Levich regimes apply.[54,59,61,62,64-68]

PS-containing antimicrobial polymer films are generally electrospun,[22,26,27] grafted onto polymers,[20-25] or immobilized on hard supports.[22,30-33] There has been limited research into solution processing coating techniques, however, spin-coating,[71] spray-coating,[71] and layer-by-layer techniques have been investigated.[16] SbQ-PVA has been used in solution processing to create an inkjet medium by solution casting, blade coating, dip-coating, and spin-coating.[72] Blade

coating was selected for this research to limit the amount of material wasted, as photosensitizers are costly, and provide introductory films that can be transitioned to slot-die coating or scaled up for manufacturing

CHAPTER 4

Experimental Methodology

4.1 Material Selection

The coatings materials were selected based off previous photoactive polymer coating studies (Figure 4.1).[12,13] The UV-photocrosslinkable polymer, *N*-methyl-4(4'-formyl-styryl)pyridinium methosulfate acetal poly(vinyl alcohol) (SbQ-PVA), containing 4.1 mol% functional SbQ groups was purchased as a 13.33 wt% aqueous solution from Polysciences, Inc. This polymer is water soluble, making it more environmentally friendly than in-soluble polymers. It undergoes photodimerization of its double bonds[73], removing the requirement of a an additional crosslinker. Anionic polymer polystyrene-sulfonic acid (PSS) was purchased from MilliporeSigma and a crosslinker (3-glycidyloxypropyl)trimethoxysilane (GOPS) was obtained from Fischer Scientific. PSS was chosen for its negative charge, used to investigate the effect of electrostatic interactions on PS leaching.

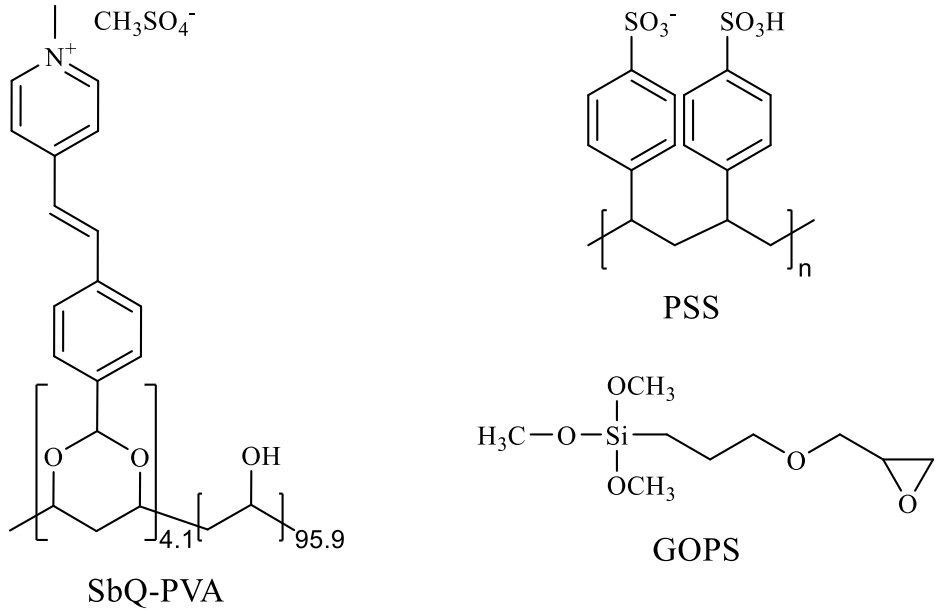

Figure 4.1 Chemical structures of photocrosslinkable SbQ-PVA and PSS with crosslinker GOPS

Comparable photosensitizers (Figure 4.2) were also used, including cationic tetra(4-*N*-methylpyridyl)porphine *p*-Toluenesulfonate ($TMPyP^{4+}$) purchased from Fischer Scientific, which has a singlet oxygen quantum yield (ϕ_Δ) of 0.75.[74,75] Cationic methylene blue (MB) and anionic rose bengal (RB) were purchased from Acros Organics and have a $\phi_\Delta = 0.66$[74] and ϕ_Δ = 0.74,[74,76] respectively. These three photosensitizers were chosen, as they are water soluble and have been shown to successfully inactivate pathogens when employed in SbQ-PVA.

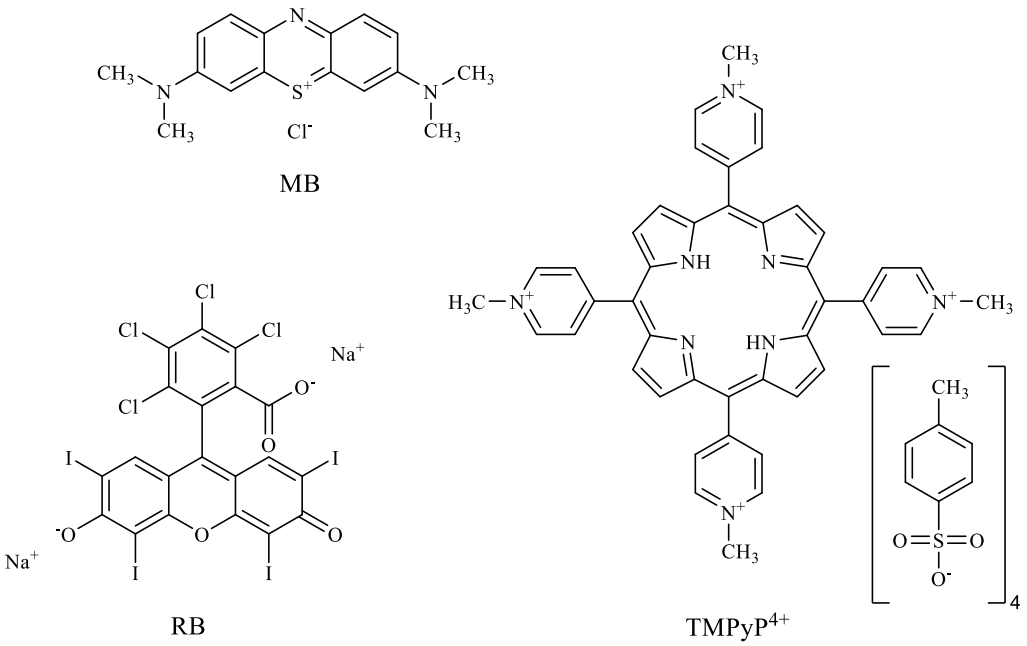

Figure 4.2 Chemical structures of cationic $TMPyP^{4+}$ and MB, and anionic RB

The first substrate used was 15x15x0.7 mm silicate glass, obtained from South China Xiangcheng Technology Co., Ltd.. The glass was successively cleaned in detergent, acetone, and isopropyl alcohol for 20 minutes in a sonicated bath. Following these steps, the glass substrates were cleaned vis UV-ozone to remove any surface hydrocarbons before coating. Glass substrates were chosen due to their availability for solution processing and the ability to take transmission

measurements of the film on them. The second substrate was 11x11x1.6 mm solid nylon, which was originally purchased from Grainger as a 12x12x0.0625 in sheet and laser cut down to size. The raised edges that were formed from the laser cutter were manually deburred. The nylon was chosen as a translational material to investigate hard substrates, as the previous studies showed good adhesion of SbQ-PVA to nylon.[12,13]

4.2 Polymer Solutions

Two different polymer solutions were studied. The first was a 4.65 wt% SbQ-PVA/water solution, to which photosensitizers were added at a 1 wt% PS/SbQ-PVA. This solution was stirred for 1 hr before use to ensure that the PS and SbQ-PVA were fully dissolved. The second was a 5.08 wt% polymer/water solution composed of 45.46 wt% PSS/SbQ-PVA and 1 vol% GOPS. 1 wt% photosensitizers were added to the polymer blends and stirred for 1 hour.

4.3 Coating Procedure

A 4.5x3.25x0.05 cm, octadecyltrichlorosilane treated silicon wafer was attached to THORLabs Benchtop Motor Mount with vacuum mount via a vacuum pump. Unless otherwise stated the coating parameters were as follows: gap height between the substrate and blade was leveled to 100 μm, the blade was set to a 45° angle to the substrate, the blade acceleration was 1000 mm/s^2, the speed was 100 mm/s, and the volume of dispensed solution was 3.5 μL. The blade was positioned 1 mm from the front edge of the substrate. The solutions were pipetted along the length of the blade to create the coating meniscus. Using the Kenesis Software, the blade was moved along the length of the substrate until it was completely coated. Then, the coated substrates placed in an Asiga Flash UV-curing box (36W, 350-400 nm) for 60 min. For

the PSS/SbQ-PVA blend coatings, they were annealed at 145° for 30 min after being UV cured. After crosslinking, all samples were washed in DI water overnight and airdried until completely dry before characterization and antimicrobial photodynamic inactivation (aPDI) assays.

4.4 Characterization

4.4.1 Profilometry

The thickness of the films was measured using a Tencor P-& Stylus Profilometer. The samples were scored with a razor blade to uncover a portion of the substrate. The height difference between the two surfaces was then calculated to obtain thicknesses.

4.4.2 Microscopy

The surface morphologies of the coated samples were examined using a Nikon Eclipse LV100N Optical Microscope from 5x to 100x magnification.

Scanning electron microscopy was also used to obstain surface micrographs. A variable-pressure Hitachi S3200N microscope equipped with an Oxford energy-dispersive X-ray spectroscopy (EDS) detector for bulk compositions analysis. The samples were mounted on aluminum stubs, and low magnification images were taken with an accelerating voltage of 20 kV and a column pressure of 30 Pa N_2.

4.4.3 Ultraviolet-visible Spectroscopy

The presence PS in the glass samples was confirmed using ultraviolet-visible spectroscopy with an optical fiber, Filmetrics light source, and FilMeasure software. Transmission data was obtained on cured films and on dry films after washing. The data obtained

in percent transmission was converted to absorbance using the Beer-Lambert Law (Equation 6), where *A* is the absorbance (abs), ε is the molar absorptivity coefficient ($M^{-1}cm^{-1}$), *l* is the pathlength (cm), and *c* is the concentration.

$$A = \varepsilon l c \tag{6}$$

Calibration curves for the photosensitizers ($TMPyP^{4+}$, MB, and RB) were created using a 105 Buck Scientific UV-Vis Spectrometer and polymethyl methacrylate (*l* = 1 cm) at λ_{max} = 421 nm, λ_{max} = 664 nm, and λ_{max} = 549 nm, respectively. The recorded absorbance for PS/water solutions from 1 uM to 20 uM were plotted against the concentrations to obtain the molar absorptivity coefficient. Samples with unknown concentration were collected from the solution used to wash the samples. The absorbances for these solutions were measured and used with the linear regressions, from the calibration curves, to calculate the concentration.

4.4.4 Antimicrobial Photodynamic Inactivation Assays

The aPDI assays were conducted using gram-positive methicillin-susceptible *S. aureus* 29213 (MRSA) with a minimum detection limit (MDL) of 0.0001% survival. Cultures were grown using 5 mL of tryptic soy broth (TSB), purchased from Teknova, at 37˚C at 250 rpm. The optical density of the bacteria was observed with a Genesys 10 UV scanning spectrophotometer at 600 nm, until they grew to an optical density of ~0.4, or a concentration of >1.0 to 4.0 x 10^8 colony-forming units per mL (CFU/mL). Cultures were centrifuged at 3374 *g* for 5 minutes, with the sequent 20 bacterial pellets were resuspended in 5 mL phosphate buffered saline (PBS), purchased from Fischer Scientific, and the supernatant fluid was disposed. Glass samples were

scored and cut down to 11x11 mm squares, same size as the nylon substrates, to fit in a 24-well plate. For illuminated plates, 3 PS-containing samples were placed in the center of a 24-well plate, and 50 uL resuspended bacterial solution was pipetted onto the center of the sample. The plate was covered with plastic wrap and placed under the LumaCare LC122 incoherent visible light source, containing an OSRAM 64653 HLX Xenophot bulb (250 W, 24 V) and LUM V fiber optic probe (400–700 nm band pass filter) with 95±3% average transmittance. An Orphir Optronics Ltd. Orion power meter was used to set the light intensity to of 65±5 mW/cm^2. Samples were illuminated for 60 min, then directly added 200 uL PBS. After mixing PBS with leftover liquid solution on samples, 40 uL liquid was took out to perform a create 6, 10-fold serial dilution. For each sample, 10 uL from each dilution was added to a 6-column-gridded square antibiotic TSB/agar plate and incubated at 37˚C overnight. The above procedure was repeated for non-illuminated 24-well plates, with 1 PS-free (light only control) sample and 2 PS-containing samples (dark control), which were covered in aluminum foil and left for 60 minutes before bacterial collection. The CFU were counted and the bacterial inactivation was calculated by dividing the CFU/mL of the dark and experimental samples by that of the PS-free control. Statistical significance was established at p-values less then 0.05, and was assessed by one-way ANOVA with Tukey's multiple comparison test.

CHAPTER 5

Results and Discussion

5.1 Blade Coating Optimization

In previous research,[12,13] the photoactive coating was applied to various textiles, focusing on applications that are high-touch fabrics in health care settings to evaluate the use of this same photoactive coating on high-touch hard surfaces, such as bedside rails and tables, IV pumps, and supply carts.[77,78] SbQ-PVA was evaluated for its coating quality using blade coating on both glass and nylon, then all three photosensitizers were evaluated for their antimicrobial efficacy.

Glass substrates were coated with both neat SbQ-PVA solutions and SbQ-PVA/PS solutions. The ideal thin film quality and thickness were obtained by varying the neat SbQ-PVA concentration in solution, the coating velocity, and the volume of dispensed coating solution. The polymer concentration was evaluated to change the viscosity of the coating solution. In agreement with solution processing literature decreasing the polymer concentration, thus decreasing the frictional forces between the meniscus and substrate, led to a decrease in dry film thickness. As-purchased SbQ-PVA solution was too viscous to pipet and dispense an even meniscus, making it unusable for making satisfactory films. The solution was diluted from the original dilution factor of 7.5 to 30 to decrease the viscosity and enable adequate coating. As seen in Figure 5.1, this decrease in solution viscosity dramatically decreased the dry SbQ-PVA film thickness. A dilution factor of 22.5 (4.44 wt% SbQ-PVA in water) was chosen as it produced film thicknesses around 200 nm. A thickness of 200 nm is within the producible realm of blade coating and allows for the diffusion of ROS to the film surface for inactivation.

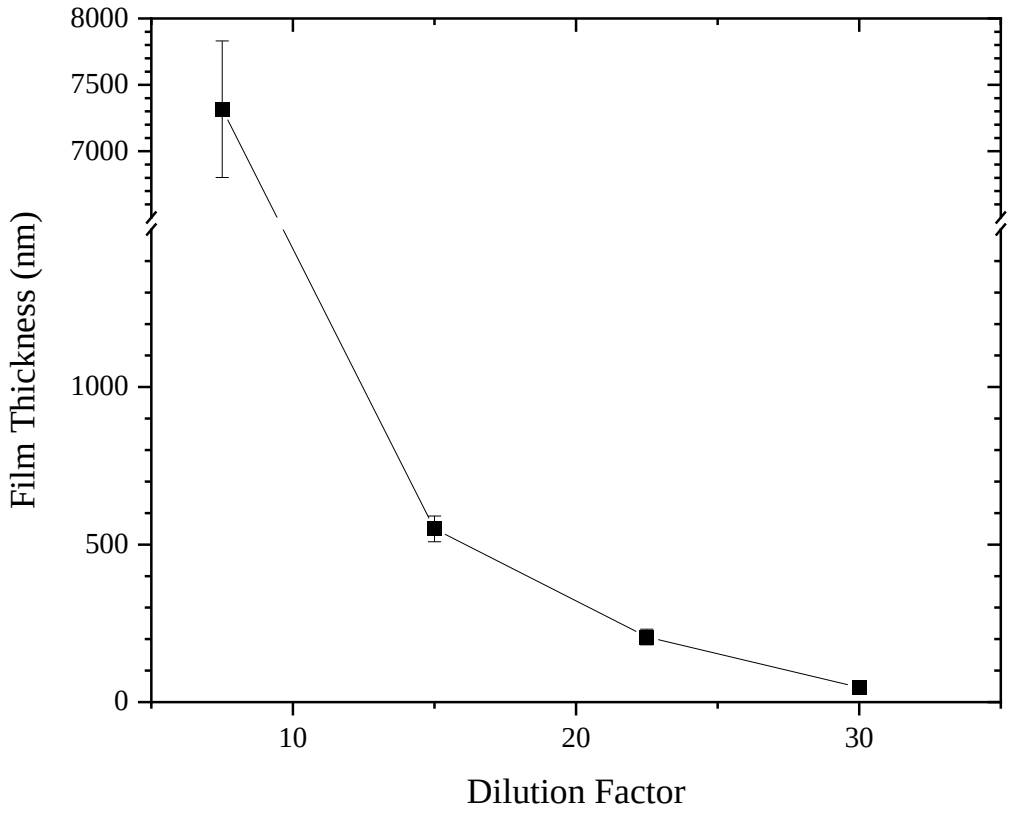

Figure 5.1 Measured film thickness as a function of dilution factor of SbQ-PVA in water (blade height = 100 μm, velocity = 1 mm/s, acceleration = 1000 mm/s^2, solution volume = 3.5 μL)

Coating velocity was also studied for its influence on the dry film thickness. Starting at a velocity of 4 mm/s, the speed was decreased by a factor of 2 until a velocity of 0.0625 mm/s was reached. The range of velocities display the compromise between evaporation and Landau-Levich regimes and their effects on film thickness. The minimum thickness was obtained at approximately 0.25 mm/s (Figure 5.2). To maintain the desired 200 nm film thickness, a speed of 1 mm/s was chosen for future samples. The faster coating time falls in the Landau-Levich regime, and allows for a coating time approximately 11 times faster than if the same-thickness velocity from the evaporation regime was used.

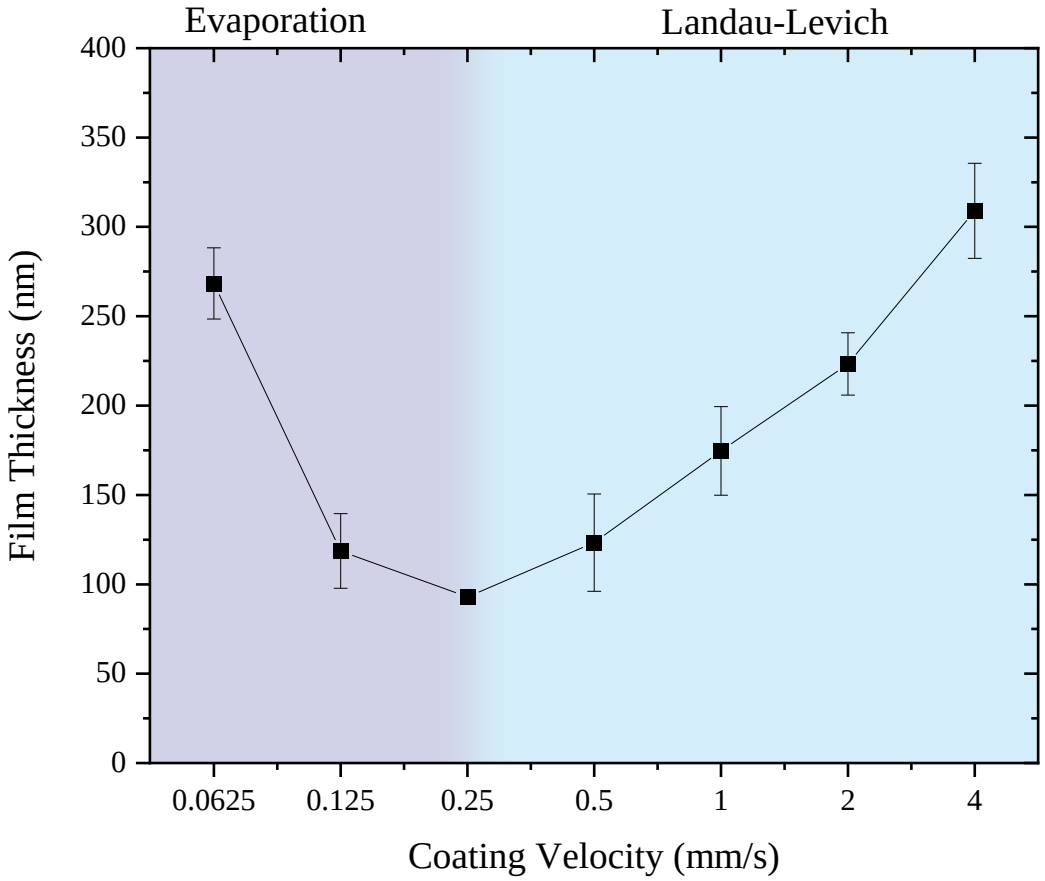

Figure 5.2 Measured film thickness as a function of coating velocity (4.65 wt% SbQ-PVA/water, blade height = 100 μm, acceleration = 1000 mm/s^2, solution volume = 3.5 μL)

The volume of dispensed solution was also investigated. A minimum solution volume was needed to make the full 15 mm meniscus across the glass substrate; however, the glass substrate was not long enough to use said minimum. A volume range of 2.5-4 μL was tested. Higher dispensed volumes tended to produce thicker films. However, the high variation can be attributed to the small difference between the volumes, thus not significantly increasing the viscous forces between the meniscus and the substrate to create a clear trend (Figure 5.3). Similar studies were done with ranges up to 70 μL and showed a distinguishable, positive relationship between thickness and solution volume. Smaller volumes were not heavy enough to

reliably release the bead of solution at the end of the pipet. A volume of 3.5 μL was arbitrarily chosen as it provided enough solution to easily pipet a meniscus.

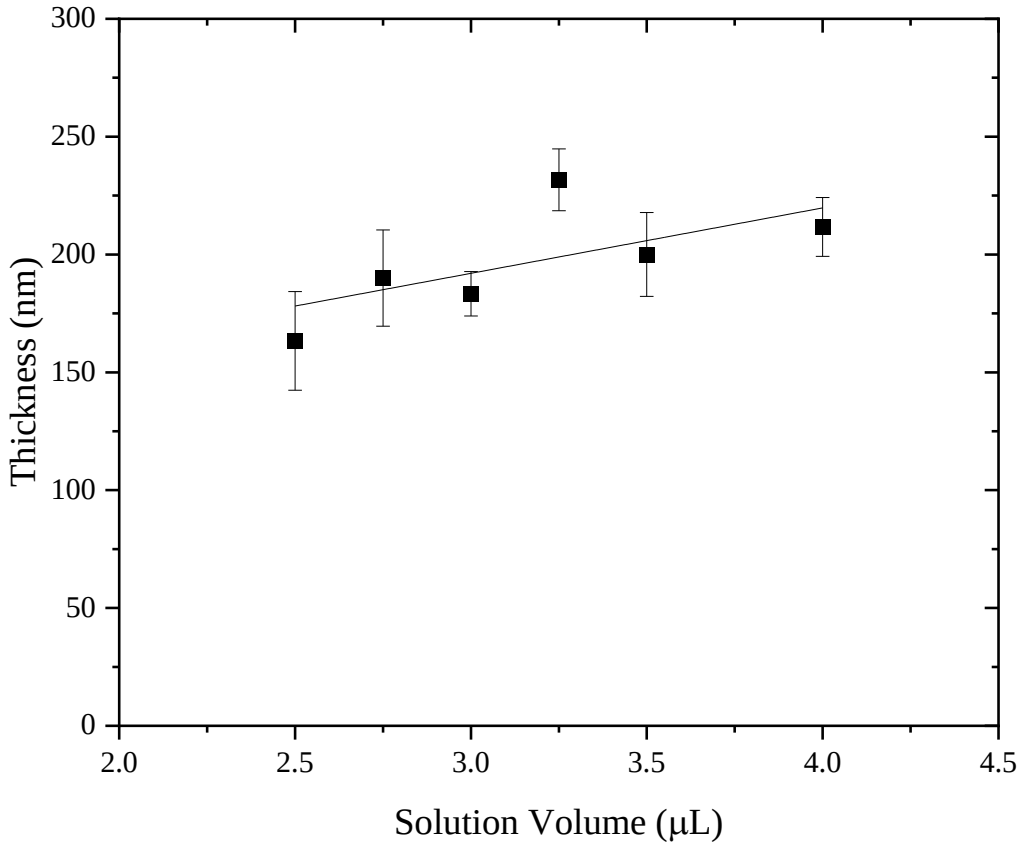

Figure 5.3. Measured film thickness as a function of solution volume (4.65 wt% SbQ-PVA/water, blade height = 100 μm, velocity = 1 mm/s, acceleration = 1000 mm/s^2)

SbQ-PVA/PS solutions were also coated onto hard Nylon 6,6 substrates. The nylon was purchased as a 12x12x0.0625-inch sheet that was laser cut into 11x11 mm squares. The edges of each substrate were raised from melting during laser cutting which did not allow for the blade to be leveled on the surface of the substrate. A deburring tool was used to remove the raised edges

on each sample. The nylon substrates were blade coated using the same parameters employed on the glass substrates.

5.2 Polymer Coating

5.2.1 Glass Substrates

The thin films were imaged using low magnification scanning electron microscopy to observe the coating surface quality. For the glass coated samples (Figure 5.4), no contrast between light and dark regions throughout the image indicates a homogeneous surface topography. EDS confirmed that the coating was present on the glass by detecting carbon.

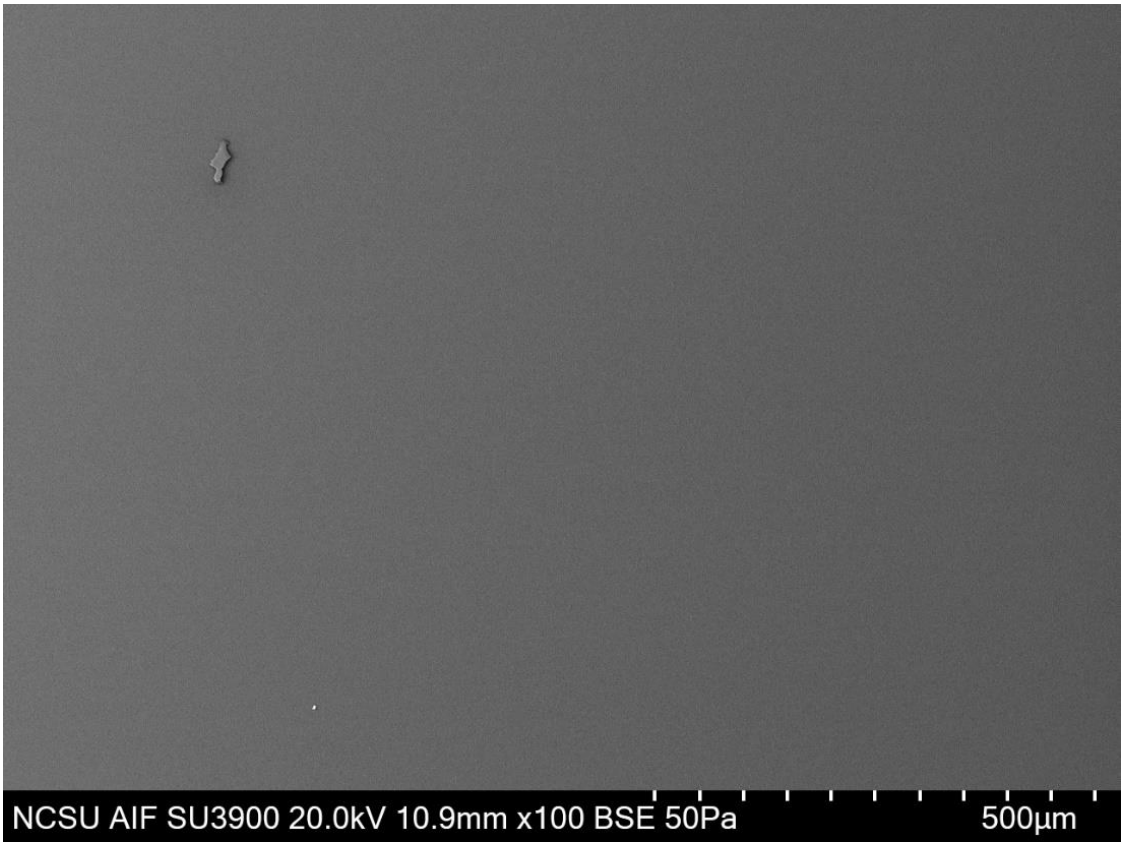

Figure 5.4 SEM image of SbQ-PVA coated on glass

The thickness measurements were performed using a surface profilometer. The SbQ-PVA films were scored, then the height difference between the coating and the glass substrate was measured to obtain the film thicknesses. The average coating thickness is approximately ~180-220 nm on the glass substrates.

The SbQ-PVA solutions were stirred for 1 hr before use to ensure that they were homogeneous. When the solutions were not mixed completely the samples did not have a homogeneous topology. They exhibited transparent circular regions surrounded by opaque film instead of the intended completely transparent, film.

To investigate both regions, the samples were viewed using an optical microscope. The opaque regions are comprised of many small polygonal regions where the internal area appears to be smooth. There should not be a separate phase in the film as the SbQ-PVA is an amorphous crosslinking polymer, ruling out phase separation as the cause of the polygonal regions. These regions have a folded appearance, indicating that they are wrinkles. This was confirmed through SEM in Figure 5.5. The lighter regions are a single layer of SbQ-PVA while the darker regions contain more material. Additionally, a smaller wrinkle can still be observed under a large fold of SbQ-PVA. The wrinkling could be due to a variation in crosslinking between poor mixed and well-mixed solutions. Solution with a higher concentration of polymer will have a higher degree of crosslinking than solutions with a lower concentration of polymer as there is more crosslinker available. For the regions with more crosslinking, there was little swelling during the washing step which allowed the film to maintain its structure. However, for the regions with less crosslinking, there was increased swelling and wetting of the glass substrate underneath the film. The rigid glass restricts the film, imparting in-plane compressive stresses which cause the film to deform and debond from the glass.[79-81]

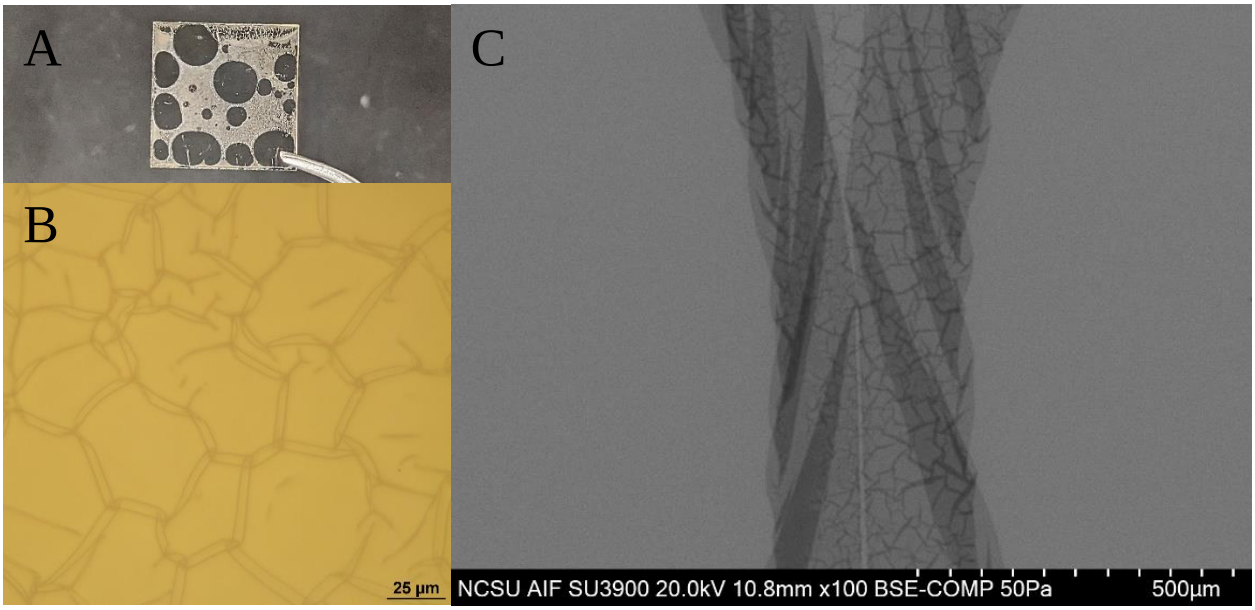

Figure 5.5 (A) Photographic, (B) optical microscopy image, and (C) SEM image of heterogenous SbQ-PVA/water solution (1 wt% loading of $TMPyP^{4+}$ to SbQ-PVA) coated on glass SEM image of SbQ-PVA coated on glass

5.2.2 Nylon Substrates

Contrast can be seen as horizontal lines across the SbQ-PVA coated nylon samples (Figure 5.6). The manufacturing process for the nylon sheet is unknown, but they were likely extruded, so the lines can be attributed to crystal orientation along the flow direction or die line defects on the nylon substrates themselves.[82] Due to this initial surface topography, the SbQ-PVA coating was not as smooth on the nylon as it was on the glass substrates. The resulting film thickness on the nylon was difficult to measure using the profilometer due to the uneven surface, the variable thickness of the substrate itself, and that the soft nylon surface. The average film thickness for the SbQ-PVA coated nylon was approximately 200 nm. The darker regions seen in Figure 16 are cracks in the substrate, which could be due to crazing or die lines created during the manufacturing process.

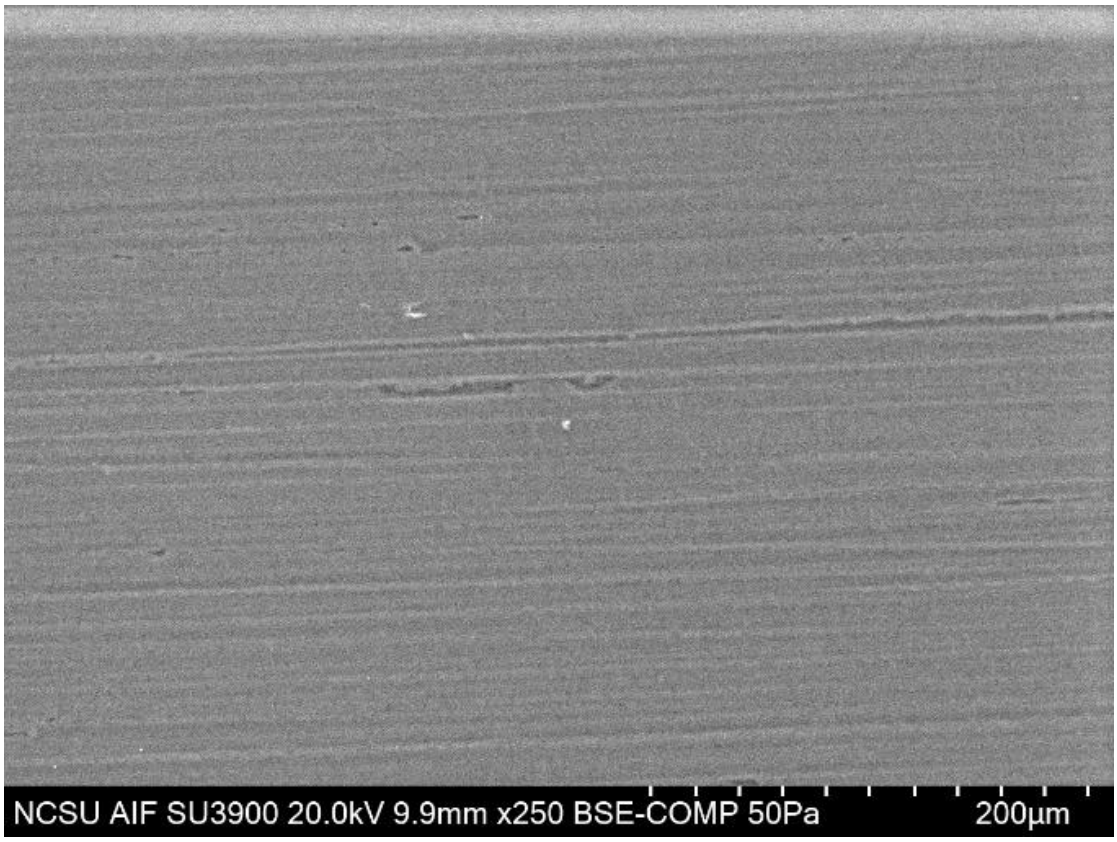

Figure 5.6 SEM image of SbQ-PVA coated on nylon

The SbQ-PVA cannot be differentiated from the nylon using EDS as they both contain the same three elements; however, the composition of carbon, oxygen, and nitrogen was different between the coated and uncoated nylon, indicating that SbQ-PVA is present.

5.3 Photosensitizer Loading

When the photosensitizers ($TMPyP^{4+}$, MB, or RB) were added to the polymer solution, the coated glass appeared pale yellow, blue, or pink, respectively (Figure 5.7). UV-Vis spectroscopy was performed on the coated glass samples to confirm the presence of the PS in the film after crosslinking. For all three spectra in Figure 5.8, a maximum is seen at approximately

350 nm, further confirming the presence of SbQ-PVA. The presence of PS is confirmed at a λ_{max} around 421 nm for $TMPyP^{4+}$, 664 nm for MB, and 549 nm for RB.

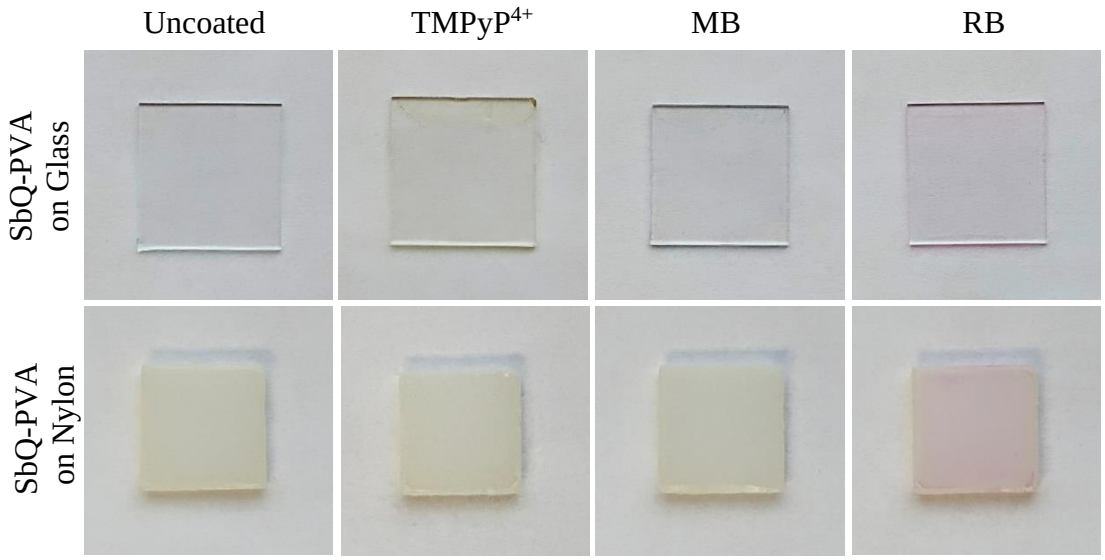

Figure 5.7 Photographic images of uncoated and PS/SbQ-PVA coated glass and nylon substrates.

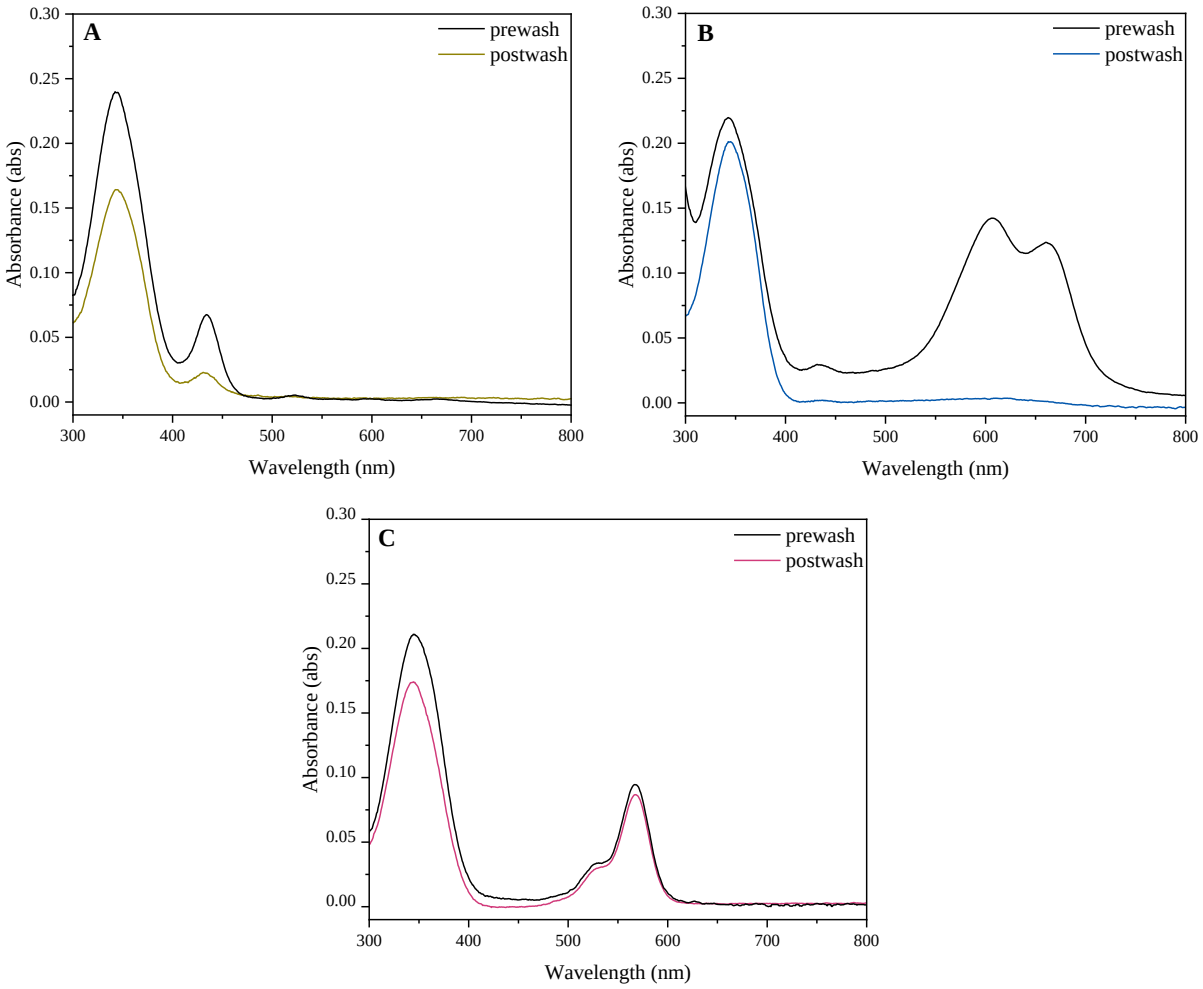

Figure 5.8. UV-Vis spectra of (A) $TMPyP^{4+}$/, (B) MB/, and (C) RB/SbQ-PVA coated glass substrates before and after washing

The samples were then washed to remove any excess photosensitizer not fully detained in the crosslinked SbQ-PVA. The two cationic polymers showed heavy leaching when washed with DI water, which was observed by a decrease in pigmentation. The anionic RB had no observable leaching from the naked eye. This is attributed to the electrostatic attraction between the positively charged methylpyridinium groups on the SbQ-PVA and the negatively PS.

Electrostatic repulsion is likely responsible for the rapid leaching of cationic $TMPyP^{4+}$ and MB, out of the crosslinked matrix when washed.

With both glass and nylon samples EDS did not detect the identifying elements for the photosensitizers. This is likely due to the low loading of the PS in the thin film and interference signals from the substrates.

For glass samples UV-Vis spectroscopy was again used to confirm the presence of the PS. The same peak locations observed before and after washing, with lower intensities after (Figure 5.8). To further investigate the amount of photosensitizer that leached from the films, UV-Vis was performed on the water solution used to wash the samples.

5.3.1 Leaching Study

To determine the concentration of PS in the washing solution calibration curves were compiled for each PS using a series of solutions with concentrations ranging from 1 uM to 20 uM. The wavelength used for measure the absorbance for each concentration was 421 nm for $TMPyP^{4+}$, 664 nm for MB, and 549 nm for RB. As expected, all three plots fit a linear regression arising from the Beer-Lambert law which allows for the molar absorptivity coefficient to be calculated (Figure 5.9). The molar absorptivity coefficient for $TMPyP^{4+}$ at 421 nm was 255,000 $M^{-1}cm^{-1}$, which agrees with coefficients measured in other studies (226,000 $M^{-1}cm^{-}1$ at 422 nm).[83] The molar absorptivity coefficient varied from values reported in the literature for MB and RB.

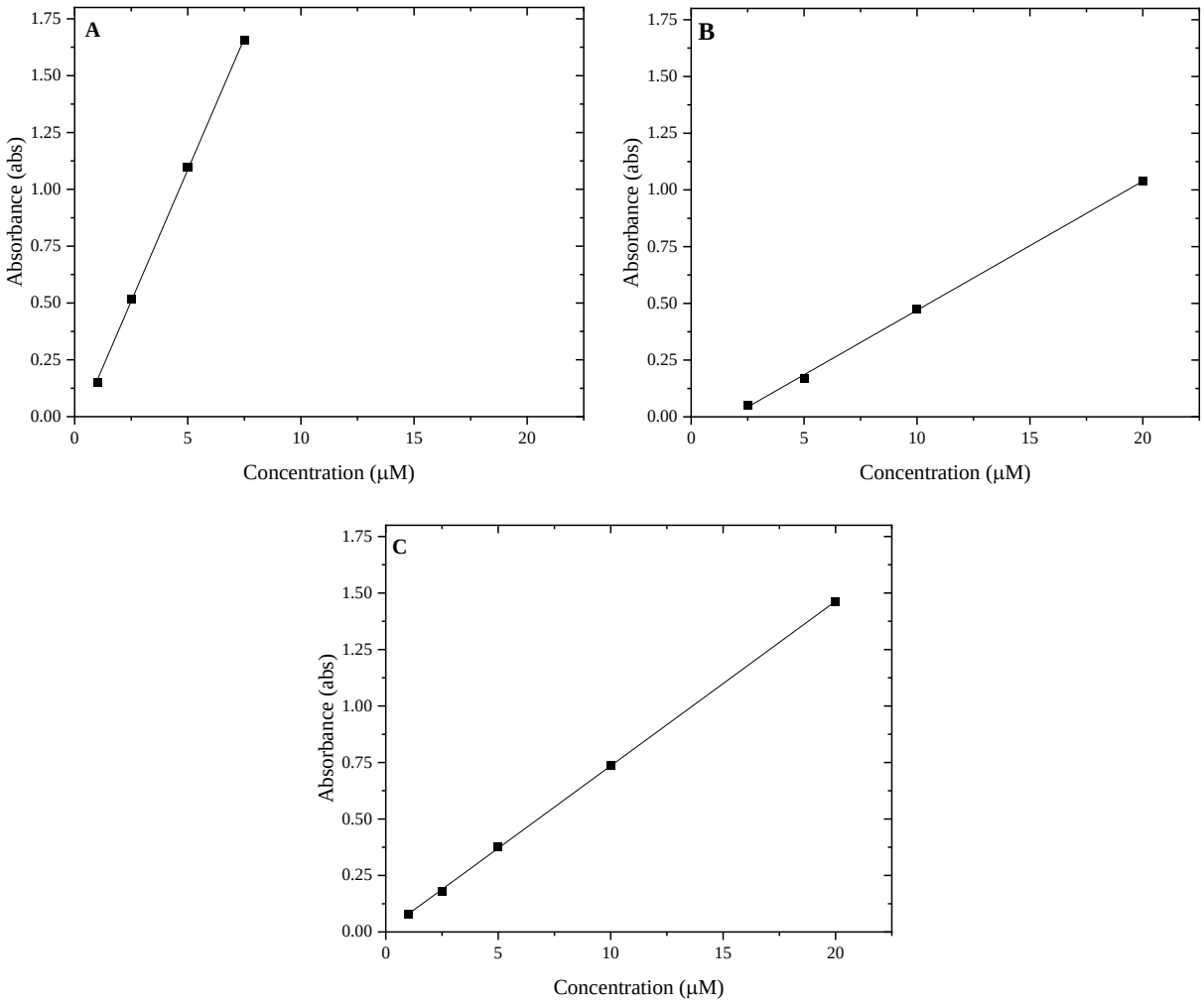

Figure 5.9 Calibration curves for (A) $TMPyP^{4+}$, (B) MB, and (C) RB in aqueous soluitons

MB can produce two different maxima according to the composition of monomers and dimers. This composition is affected by the concentration of MB in solution, with higher concentrations having increasing dimer amounts.[84,85] Solutions under 7 μM in water have a predominantly monomer composition, creating a maximum at 664 nm and a molar absorption coefficient of 95,000 $M^{-1}cm^{-}1$.[84-86] However, at concentrations higher than this the dimers create a maximum of around 600 nm and decrease the molar absorption coefficient at λ_{max} = 664 nm.[84-86] The measured coefficient from this study was 57,000 $M^{-1}cm^{-1}$, which is significantly lower

than typically reported in literature.[84-86] However, there are studies that have reported similar numbers (~56,600 $M^{-1}cm^{-1}$) when using solutions at higher concentrations.[87] The molar absorptivity coefficient for RB was calculated to be 73,000 $M^{-1}cm^{-1}$ at 549 nm, which is lower than the literature value ~98,000 $M^{-1}cm^{-1}$.[88,89] RB also forms dimers at higher concentrations, but the threshold of 10 mM was not used in this research, therefore monomer-dimer concentrations can be ignored.[63,89]

A lower molar absorptivity means that the transition between the ground state and excited state of the PS is less favorable, resulting in a lower absorbance and lower ROS prodcution. A high molar absorptivity is critical to maximize the absorbance of light in PS-containing polymer coatings. An infinitely thick film for complete absorbance is not applicable to photosensitizers because the diffusion of singlet oxygen in aqueous environments is only several hundred nanometers. Therefore, a PS is needed that has high molar absorptivity to maximize the absorbance at lower light quantities. Additionally, the PS should have a high singlet oxygen quantum yield so that excitation of the PS is created a high amount of singlet oxygen compared to other ROS. For the PS used in this study, it is expected that $TMPyP^{4+}$ should perform the best as it had both the highest molar absorptivity and one of the highest singlet oxygen quantum yield of 0.74.[74,75] $TMPyP^{4+}$ would be followed by RB with a singlet oxygen quantum yield of 0.74,[74,76] then MB with a quantum yield of 0.66.[74]

The PS/SbQ-PVA glass and nylon samples were washed overnight in DI water, followed by the subsequent collection of each leachant. The leachant samples were analyzed spectroscopically at their PS specific λ_{max} to measure absorbance. The concentration of each leachant sample was calculated using the calibrate curves and Beer-Lambert Law (Table 5.1). The concentration of PS in the $TMPyP^{4+}$ and RB leachant samples were below the limit of

accurate detection for the study for both coated glass and nylon. The MB leachant samples had the highest concentration in solution, however, it was close to the lower limit of the study. For all three PS the concentration measured for their respective leachant samples was very low compared to the concentration of the coating solution.

Table 5.1 PS concentrations (μM) coating and leachant samples

PS	Coating solution	Leachant samples from coated glass	Leachant samples from coated nylon
$TMPyP^{4+}$	341.1	0.187* ± 0.004	0.179* ± 0.003
MB	1454	1.228 ± 0.075	1.204 ± 0.032
RB	457.1	-0.041* ± 0.008	-0.055* ± 0.024

* Value lies below the limit of accurate detection for the study (1 μM)

5.3.2 PSS/SbQ-PVA Blend

An anionic polymer was investigated to investigate leaching of the cationic PS. A PSS/GOPS solution was combined with both a $TMPyP^{4+}$/SbQ-PVA and MB/SbQ-PVA solutions and coating parameters on glass as described in Sections 4.2 and 4.3, respectively. The samples were cured for 1 hr under UV light then annealed at 145˚C for 30 minutes to crosslink the PSS and GOPS. The resulting network polymer coating should have better adherence to the glass, less swelling due to increased crosslinking, and better retention of the PS with the negatively charged sulfonate ions. The GOPS adheres the PSS to the glass through bonding between the hydroxyl groups on the glass and methoxysilane groups on the GOPS.[90-92] This combats the delamination of the SbQ-PVA due to swelling. The PSS is crosslinked with the GOPS due to bonding between the sulfonic acid groups on the PSS and the epoxy ring on the GOPS.[90-92] Increasing the

crosslinking will decrease the amount of swelling that occurs during washing, hindering both delamination and wrinkling. Additionally, the sulfonic acid groups on the PSS and the hydroxyl groups on the PVA backbone can be polymerized during the annealing step.[93-95] It is expected that the higher levels of crosslinking could aid the anionic sulfonate ions in retaining the PS by trapping the molecules within the polymer network.

PSS/SbQ-PVA network polymer samples were made with the same coating parameters as the SbQ-PVA samples. They were much thinner than the SbQ-PVA samples at approximately 55 nm. However, there was no visible leaching of the cationic dyes after washing (Figure 5.10). Unfortunately, this polymer network was unable to be used after the initial investigation as the two charged long-chain polymers started to entangle and precipitate out of solution.

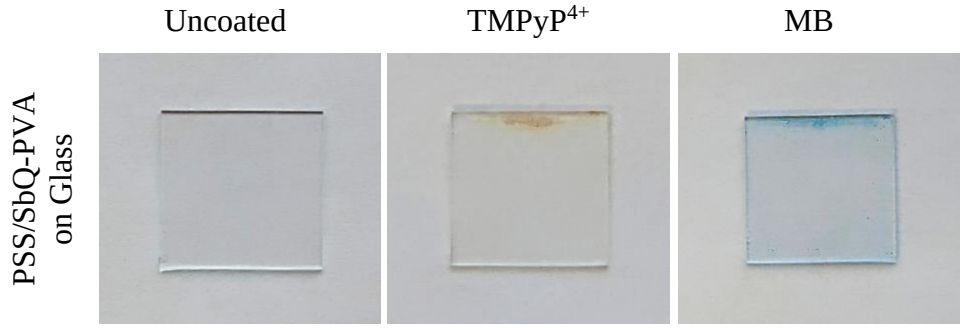

Figure 5.10 Photographic images of uncoated and PS/PSS/SbQ-PVA coated glass

5.4 Antibacterial Behavior

The aPDI assays were performed at the conditions stated in section 4.4.4, which have been used in previous PS/SbQ-PVA studies, as the illumination parameters alone are not able to inactivate the employed bacteria.[12,13,24,25] The percent survival of MRSA was compared between PS-free (light control), non-illuminated PS/SbQ-PVA samples (dark controls), and illuminated

PS/SbQ-PVA samples (Figure 5.11). The PS-Free samples, which were used as a baseline for the comparison of the PS-containing samples, and the dark controls did not show significant inactivation. Therefore, the use of a PS in combination with illumination is needed for bacterial inactivation. Not all the illuminated PS/SbQ-PVA samples showed a statistically significant reduction of MRSA, which will be discussed further. The coated glass and nylon samples showed a CFU/mL reduction ranging from 33.333% to 99.88%.

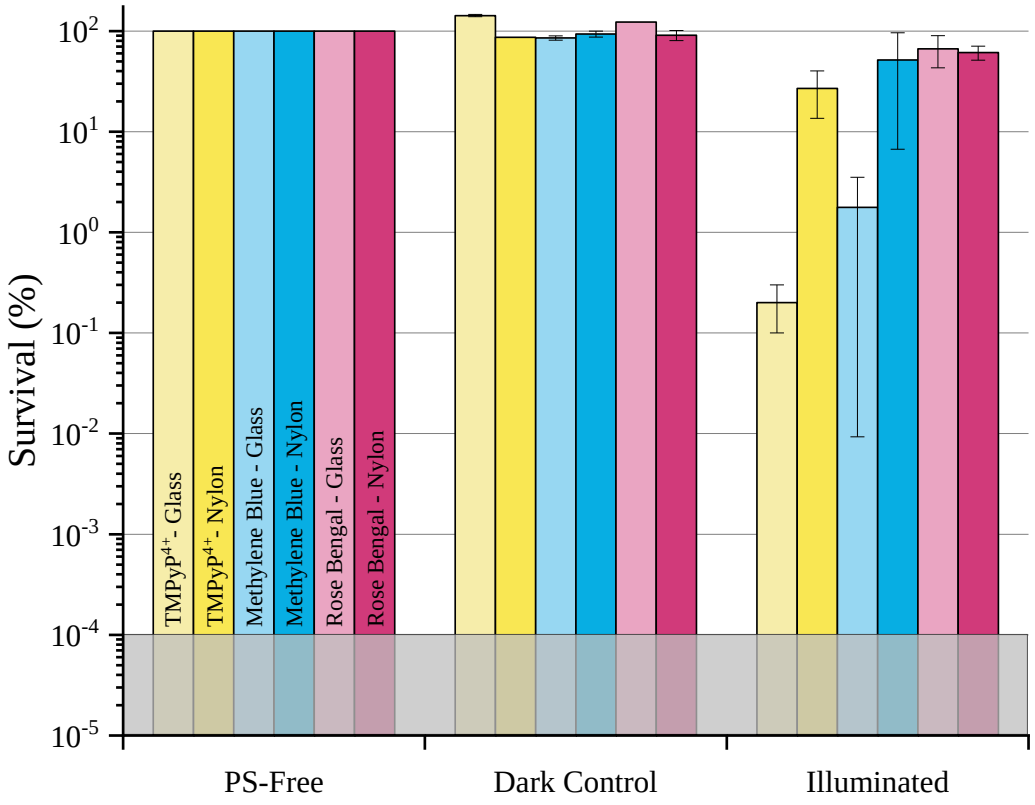

Figure 5.11 Antimicrobial photodynamic inactivation efficacy of glass and nylon substrates coated with PS/SbQ-PVA for MRSA The grey shaded region represent the MDL for each study.

For the $TMPyP^{4+}$/SbQ-PVA coated samples a one-way ANOVA revealed that there was a statistically significant difference between the percent survival of MRSA between at least two

test conditions for both the coated glass ($F(2,3) = [3094.816]$, $p < 0.001$) and nylon ($F(2,3) = [146.807]$, $p = 0.001$). For coated glass substrates all three testing conditions showed significant differences in antibacterial activity, as determined by a Tukey's test. The dark controls for $TMPyP^{4+}$/SbQ-PVA coated on glass substrates had an ~142.5% increase in bacterial survival as compared to the light only control ($p < 0.001$). For the experimental condition, there was a 99.8% (~2.9 log units) reduction of CFU/mL, which was statistically significant from both the light ($p < 0.001$) and dark ($p < 0.001$) controls. The coated nylon samples did not show any significant antibacterial activity compared to the light controls ($p = 0.16$), however, the experimental condition showed statistically significant inactivation (68.16%, ~0.8 log units, $p = 0.002$) compared to the light and dark controls.

In the MB/SbQ-PVA coated samples there were significant differences in antibacterial activity on the glass substrates ($F(2,3) = [758.194]$, $p < 0.001$) between at least two experimental conditions, but not on the nylon substrates ($F(2,3) = [1.094]$, $p = 0.44$). Similarly to the $TMPyP^{4+}$/SbQ-PVA coated glass the illuminated samples had an inactivation of 98.232% (~1.9 log units, $p < 0.001$). However, the dark controls did have an inactivation of 14.706% (~0.2 log units, $p = 0.047$), which was statistically significant from the light controls. A ~0.2 log unit inactivation of bacteria is not a save level of inactivation for use, however the low variance between dark controls aided to the statistical significance. Despite this slight inactivation, the experimental condition still had significant antibacterial activity to the dark controls. It should be noted that the inactivation was 48.473% (~0.5 log units) for the MB/SbQ-PVA coated nylon samples.

The RB/SbQ-PVA coated samples had a statistically significant differences in antibacterial inactivation coated on glass ($F(2,3) = [7.214]$, $p = 0.047$) between at least two

experimental conditions, but not on the nylon substrates ($F(2,3) = [8.249]$, $p = 0.06$). The glass substrates showed an inactivation of 33.333% (~0.4 log unites), which was only statistically different than the dark controls ($p = 0.044$). The dark controls demonstrated increased 123% MRSA survival from the light controls. To note, the inactivation of RB/SbQ-PVA on nylon was 38.889% (~0.4 log units), despite its insignificant difference from the controls.

$TMPyP^{4+}$ had the highest inactivation of MRSA which can be attributed to having an experimental molar absorptivity ~3.5x to 4.5x greater than that of RB and MB, respectively. At the same loading percent, the high molar absorptivity allows the $TMPyP^{4+}$ to absorb more radiation than the other two PS, and produce an increased amount of singlet oxygen. The lack of significant inactivation from the RB/SbQ-PVA coating is likely influenced by its electrostatic interaction with the bacteria. For active antimicrobial coatings a positively charged surface is needed to attract the negatively charged cell wall to the coating for inactivation. The two cationic photosensitizers, $TMPyP^{4+}$ and MB, should aid in the attachment of MRSA to the antibacterial coating. However, RB is anionic, which will attempt to repel the bacteria from the polymer surface, decreasing its efficacy as the singlet oxygen cannot reach the unattached bacteria due to its low diffusion distance. Altogether, the higher efficacy of $TMPyP^{4+}$ is consistent with previous aPDI research using a comparable porphyrin (child compound $ZnTMPyP^{4+}$) and MB and RB.

The PS/SbQ-PVA coated glass samples performed better than their nylon counterparts, except for the RB/SbQ-PVA coatings. This is likely due to the different dye-substrate interactions between glass and nylon, most notably the ability of nylon to be dyed.[52,96-98] Similarly to wool, nylon is easily dyed by acid dyes due to ionic interactions between the protonated amine groups on the nylon and the negatively charged dye molecule.[98] Additionally, basic dyes can be used on polyamides by interacting with a carboxylate group.[52,96-98] After

coating, the photosensitizers may settle at the nylon/SbQ-PVA interface due to these attractive forces, increasing the distance that the singlet oxygen will have to travel to the surface. Thicker SbQ-PVA regions additionally have this issue. Furthermore, the uneven surface of the nylon substrates did not allow for a completely flat coating.

Similar PS/SbQ-PVA studies performed on textiles showed a 1-2 log unit increase in MRSA inactivation for each of these photosensitizers from the above-mentioned results.[13] This is most likely due to the increase surface area of antimicrobial coating on the 3D fibrous substrates, allowing for increased contact between the bacteria and coating surface. PS loading cannot be reasonably compared to other photosensitizer-containing textiles (i.e., nmol/mg of material)[12,13,20,24-27,29,33] due to the difference in substrate materials.

The antimicrobial efficacy was also evaluated for the PS/PSS/SbQ-PVA coated glass samples (Figure 5.12). The $TMPyP^{4+}$/PSS/SbQ-PVA samples showed no significant difference in antibacterial activity ($F(2,3) = [0.481]$, $p = 0.659$) between the testing conditions. Conversely, the MB/PSS/SbQ-PVA samples did show statistically significant activity ($F(2,3) = [961.657]$, $p < 0.001$) between conditions. The illuminated samples displayed an inactivation of 99.972% (~3.8 log units, $p < 0.001$), which was 2 log units more than the MB/SbQ-PVA samples. This is attributed to the assumed decrease in leached MB despite the decrease in film thickness. To provide a rationale for the lack of inactivation from the $TMPyP^{4+}$/PSS/SbQ-PVA samples, further investigation is needed.

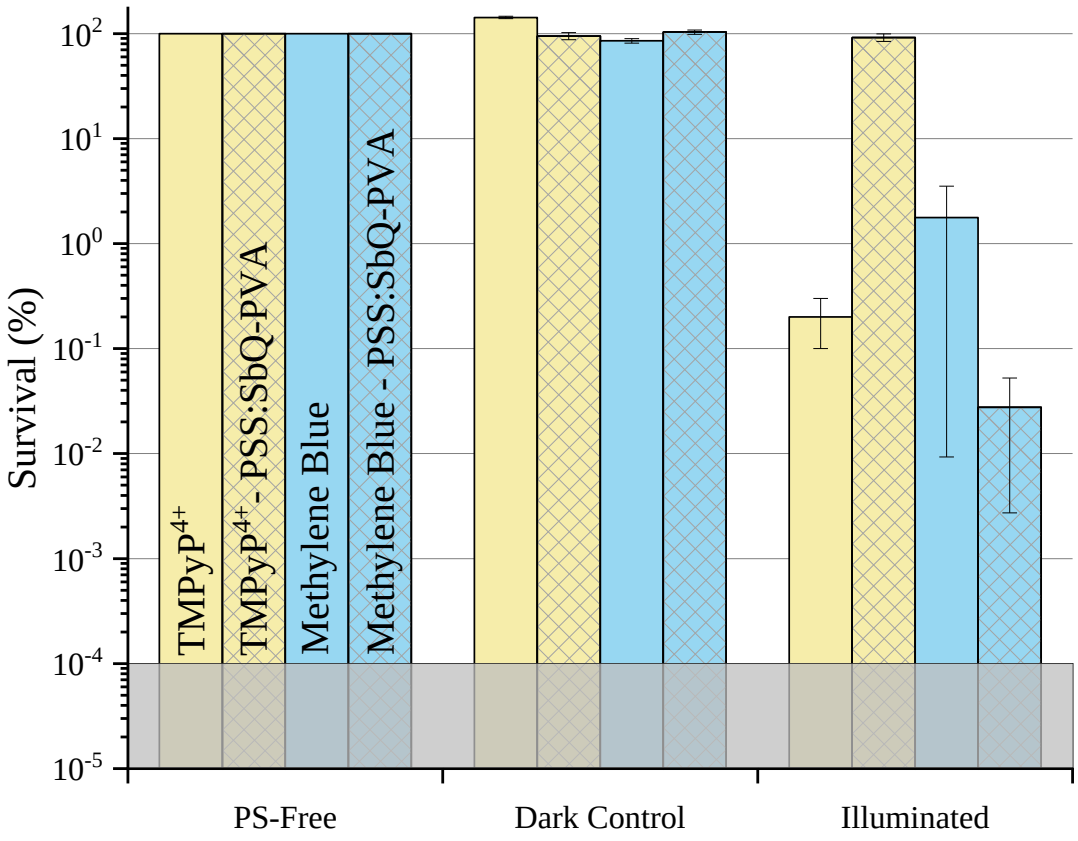

Figure 5.12 Antimicrobial photodynamic inactivation efficacy of glass substrates coated with PS/SbQ-PVA pr PS/PSS/SbQ-PVA for MRSA The grey shaded region represent the MDL for each study.

CHAPTER 6

Conclusions and Future Work

6.1 Conclusions

To conclude, the results from this introductory study demonstrate that the use of PS-containing polymer is promising for use as antimicrobial hard-surface coatings. Successful blade coating of PS/SbQ-PVA solutions shows the scalability of these materials to be coated on non-porous surfaces using a multitude of practiced meniscus-based coating techniques. While low, the antibacterial activity recordings serve as a starting point for the efficacy of PS-containing polymer films. For applications in health care settings, any level of additional antimicrobial activity will help protect those who may encounter contaminated surfaces. This research on photodynamic films serves as the beginning steps to providing increased protection, from both nosocomial infections and airborne pathogens, for healthcare workers, their patients, and the general public.

6.2 Future Work

A comprehensive range of both non-porous and porous surfaces should be tested regarding the polymer coating. These should include common high traffic hospital surface materials and are not limited to: aluminum, stainless steel, high-density polyethylene, polycarbonate, polypropylene, polyvinyl chloride, and laminate. This will confirm if photodynamic polymer coatings are truly viable on a wide range of hard surfaces. Next, the entanglement of PSS and SbQ-PVA or additional anionic/cationic polymer blends should be investigated. Working networks that further retain the cationic PS will allow for lower loadings,

thus increasing the cost of materials. Durability and longevity studies should be conducted to determine if these films can withstand long-term use on highly trafficked surfaces.

To improve the antimicrobial activity of the polymer coating, a higher photosensitizer loading can be explored. This should increase absorbance and the amount of ROS produced for killing pathogens. A higher wattage can be used in aPDI studies to provide similar results. These films should be tested against a gram-negative bacterium, an enveloped virus, and a non-enveloped virus. aPDI results using pathogens with different outer membranes (or lack thereof) and protein layers will allow for the work to translate to other HAI pathogens and viruses.[12,13,20,23,27,53]

REFERENCES

1. Pullangott, G., Kannan, U., S., G., Kiran, D. V. & Maliyekkal, S. M. A comprehensive review on antimicrobial face masks: an emerging weapon in fighting pandemics. RSC Adv. 11, 6544–6576 (2021).

2. Covid19.who.int. 2022. WHO Coronavirus (COVID-19) Dashboard. Available at: https://covid19.who.int/ (Accessed: 1st March 2022).

3. Weber, D. J., Rutala, W. A., Miller, M. B., Huslage, K. & Sickbert-Bennett, E. Role of hospital surfaces in the transmission of emerging health care-associated pathogens: Norovirus, Clostridium difficile, and Acinetobacter species. American Journal of Infection Control 38, S25–S33 (2010).

4. Kramer, A., Schwebke, I. & Kampf, G. How long do nosocomial pathogens persist on inanimate surfaces? A systematic review. BMC Infect Dis 6, 130 (2006).

5. Klevens, R. M. et al. Estimating Health Care-Associated Infections and Deaths in U.S. Hospitals, 2002. Public Health Rep 122, 160–166 (2007).

6. Magill, S. S. et al. Multistate Point-Prevalence Survey of Health Care–Associated Infections. N Engl J Med 370, 1198–1208 (2014).

7. Weiner-Lastinger, L. M. et al. The impact of coronavirus disease 2019 (COVID-19) on healthcare-associated infections in 2020: A summary of data reported to the National Healthcare Safety Network. Infect. Control Hosp. Epidemiol. 43, 12–25 (2022).

8. Neely, A. N. & Maley, M. P. Survival of enterococci and staphylococci on hospital fabrics and plastic. J Clin Microbiol 38, 724–726 (2000).

9. Morgan, D. J., Lomotan, L. L., Agnes, K., McGrail, L. & Roghmann, M.-C. Characteristics of Healthcare-Associated Infections Contributing to Unexpected In-Hospital Deaths. Infect. Control Hosp. Epidemiol. 31, 864–866 (2010).

10. Boucher, H. W. et al. Bad Bugs, No Drugs: No ESKAPE! An Update from the Infectious Diseases Society of America. CLIN INFECT DIS 48, 1–12 (2009).

11. Kamaruzzaman, N. F. et al. Antimicrobial Polymers: The Potential Replacement of Existing Antibiotics? IJMS 20, 2747 (2019).

12. Peddinti, B. S. T. et al. Photodynamic Coatings on Polymer Microfibers for Pathogen Inactivation: Effects of Application Method and Composition. ACS Appl. Mater. Interfaces 13, 155–163 (2021).

13. Ghareeb, C. R. et al. Toward Universal Photodynamic Coatings for Infection Control. Front. Med. 8, 657837 (2021).

14. Joshi, R. & Taylor, E. Contact Transmission, Part 2: Materials, Design, and Cleaning. 23 https://www.healthdesign.org/insights-solutions/contact-transmission-part-2-materials-design-and-cleaning (2019).

15. Huang, K.-S. et al. Recent Advances in Antimicrobial Polymers: A Mini-Review. IJMS 17, 1578 (2016).

16. Siedenbiedel, F. & Tiller, J. C. Antimicrobial Polymers in Solution and on Surfaces: Overview and Functional Principles. Polymers 4, 46–71 (2012).

17. Salwiczek, M. et al. Emerging rules for effective antimicrobial coatings. Trends in Biotechnology 32, 82–90 (2014).

18. Chen, A., Peng, H., Blakey, I. & Whittaker, A. K. Biocidal Polymers: A Mechanistic Overview. Polymer Reviews 57, 276–310 (2017).

19. Santos, M. et al. Recent Developments in Antimicrobial Polymers: A Review. Materials 9, 599 (2016).

20. Carpenter, B. L. et al. Synthesis, Characterization, and Antimicrobial Efficacy of Photomicrobicidal Cellulose Paper. Biomacromolecules 16, 2482–2492 (2015).

21. Mbakidi, J.-P. et al. Synthesis and photobiocidal properties of cationic porphyrin-grafted paper. Carbohydrate Polymers 91, 333–338 (2013).

22. Spagnul, C., Turner, L. C. & Boyle, R. W. Immobilized photosensitizers for antimicrobial applications. Journal of Photochemistry and Photobiology B: Biology 150, 11–30 (2015).

23. Alvarado, D. R., Argyropoulos, D. S., Scholle, F., Peddinti, B. S. T. & Ghiladi, R. A. A facile strategy for photoactive nanocellulose-based antimicrobial materials. Green Chem. 21, 3424–3435 (2019).

24. Carpenter, B. L., Feese, E., Sadeghifar, H., Argyropoulos, D. S. & Ghiladi, R. A. Porphyrin-Cellulose Nanocrystals: A Photobactericidal Material that Exhibits Broad Spectrum Antimicrobial Activity†. Photochemistry and Photobiology 88, 527–536 (2012).

25. Feese, E., Sadeghifar, H., Gracz, H. S., Argyropoulos, D. S. & Ghiladi, R. A. Photobactericidal Porphyrin-Cellulose Nanocrystals: Synthesis, Characterization, and Antimicrobial Properties. Biomacromolecules 12, 3528–3539 (2011).

26. Stoll, K. R., Scholle, F., Zhu, J., Zhang, X. & Ghiladi, R. A. BODIPY-embedded electrospun materials in antimicrobial photodynamic inactivation. Photochem. Photobiol. Sci. 18, 1923–1932 (2019).

27. Stanley, S. et al. Photosensitizer-Embedded Polyacrylonitrile Nanofibers as Antimicrobial Non-Woven Textile. Nanomaterials 6, 77 (2016).

28. Chen, W. et al. Photooxidation Properties of Photosensitizer/Direct Dye Patterned Polyester/Cotton Fabrics. Fibers Polym 19, 1687–1693 (2018).

29. Chen, W. et al. Wool/Acrylic Blended Fabrics as Next-Generation Photodynamic Antimicrobial Materials. ACS Appl. Mater. Interfaces 11, 29557–29568 (2019).

30. Felgenträger, A., Maisch, T., Späth, A., Schröder, J. A. & Bäumler, W. Singlet oxygen generation in porphyrin-doped polymeric surface coating enables antimicrobial effects on Staphylococcus aureus. Phys. Chem. Chem. Phys. 16, 20598–20607 (2014).

31. Noimark, S., Allan, E. & Parkin, I. P. Light-activated antimicrobial surfaces with enhanced efficacy induced by a dark-activated mechanism. Chem. Sci. 5, 2216–2223 (2014).

32. Decraene, V., Pratten, J. & Wilson, M. Cellulose Acetate Containing Toluidine Blue and Rose Bengal Is an Effective Antimicrobial Coating when Exposed to White Light. Appl Environ Microbiol 72, 4436–4439 (2006).

33. Dong, J., Ghiladi, R. A., Wang, Q., Cai, Y. & Wei, Q. Protoporphyrin-IX conjugated cellulose nanofibers that exhibit high antibacterial photodynamic inactivation efficacy. Nanotechnology 29, 265601 (2018).

34. Dai, T. et al. Concepts and Principles of Photodynamic Therapy as an Alternative Antifungal Discovery Platform. Front. Microbio. 3, (2012).

35. Hamblin, M. R. Photodynamic Therapy and Photobiomodulation: Can All Diseases be Treated with Light? in Encyclopedia of Modern Optics 100–135 (Elsevier, 2018). doi:10.1016/B978-0-12-803581-8.09688-0.

36. Hamblin, M. R. Antimicrobial photodynamic inactivation: a bright new technique to kill resistant microbes. Current Opinion in Microbiology 33, 67–73 (2016).

37. Kashef, N., Huang, Y.-Y. & Hamblin, M. R. Advances in antimicrobial photodynamic inactivation at the nanoscale. Nanophotonics 6, 853–879 (2017).

38. Ni, J., Wang, Y., Zhang, H., Sun, J. Z. & Tang, B. Z. Aggregation-Induced Generation of Reactive Oxygen Species: Mechanism and Photosensitizer Construction. Molecules 26, 268 (2021).

39. Dąbrowski, J. M. Reactive Oxygen Species in Photodynamic Therapy: Mechanisms of Their Generation and Potentiation. in Advances in Inorganic Chemistry vol. 70 343–394 (Elsevier, 2017).

40. Dave, D., Desai, U. & Despande, N. Photodynamic Therapy: A View through Light. JOFR 2, 82–86 (2012).

41. Fekrazad, R., Nejat, A. & Kalhori, K. A. M. Antimicrobial Photodynamic Therapy With Nanoparticles Versus Conventional Photosensitizer in Oral Diseases. in Nanostructures for Antimicrobial Therapy 237–259 (Elsevier, 2017). doi:10.1016/B978-0-323-46152-8.00010-X.

42. Grabow, W. W. Method For Determination Of Singlet Oxygen Quantum Yields For New Fluorene-based Photosensitizers In Aqueous Media For The Advancement Of Photodynamic Therapy. 87.

43. Vileno, B. et al. Singlet oxygen (1 Δ g)-mediated oxidation of cellular and subcellular components: ESR and AFM assays. J. Phys.: Condens. Matter 17, S1471–S1482 (2005).

44. Midden, W. R. & Wang, S. Y. Singlet oxygen generation for solution kinetics: clean and simple. J. Am. Chem. Soc. 105, 4129–4135 (1983).

45. Tuson, H. H. & Weibel, D. B. Bacteria–surface interactions. Soft Matter 9, 4368 (2013).

46. Yin, R. et al. Antimicrobial photodynamic inactivation in nanomedicine: small light strides against bad bugs. Nanomedicine (Lond) 10, 2379–2404 (2015).

47. Wikene, K. O., Hegge, A. B., Bruzell, E. & Tønnesen, H. H. Formulation and characterization of lyophilized curcumin solid dispersions for antimicrobial photodynamic therapy (aPDT): studies on curcumin and curcuminoids LII. Drug Dev Ind Pharm 41, 969–977 (2015).

48. Iyer, R., Wolf, J., Zhukova, D., Padanilam, D. & Nguyen, K. T. Nanomaterial Based Photo-Triggered Drug Delivery Strategies for Cancer Theranostics. in Handbook of Nanomaterials for Cancer Theranostics 351–391 (Elsevier, 2018). doi:10.1016/B978-0-12-813339-2.00012-8.

49. Xuan, W. et al. Antimicrobial Photodynamic Inactivation Mediated by Tetracyclines in Vitro and in Vivo: Photochemical Mechanisms and Potentiation by Potassium Iodide. Sci Rep 8, 17130 (2018).

50. Lange, N., Szlasa, W., Saczko, J. & Chwiłkowska, A. Potential of Cyanine Derived Dyes in Photodynamic Therapy. Pharmaceutics 13, 818 (2021).

51. Hassan, M. M. Antimicrobial Coatings for Textiles. in Handbook of Antimicrobial Coatings 321–355 (Elsevier, 2018). doi:10.1016/B978-0-12-811982-2.00016-0.

52. Andrade-Guel, M. et al. Non-Woven Fabrics Based on Nanocomposite Nylon 6/ZnO Obtained by Ultrasound-Assisted Extrusion for Improved Antimicrobial and Adsorption Methylene Blue Dye Properties. Polymers 13, 1888 (2021).

53. Jiang, C., Scholle, F. & Ghiladi, R. A. Mn-doped Zn/S quantum dots as photosensitizers for antimicrobial photodynamic inactivation. in Photonic Diagnosis and Treatment of Infections and Inflammatory Diseases II (eds. Dai, T., Wu, M. X. & Popp, J.) 25 (SPIE, 2019). doi:10.1117/12.2510934.

54. Francis, L. F. & Roberts, C. C. Dispersion and Solution Processes. in Materials Processing 415–512 (Elsevier, 2016).

55. Flory, P. J. Thermodynamics of High Polymer Solutions. The Journal of Chemical Physics 10, 51–61 (1942).

56. Huggins, M. L. Solutions of Long Chain Compounds. The Journal of Chemical Physics 9, 440–440 (1941).

57. Negi, V., Wodo, O., van Franeker, J. J., Janssen, R. A. J. & Bobbert, P. A. Simulating Phase Separation during Spin Coating of a Polymer–Fullerene Blend: A Joint Computational and Experimental Investigation. ACS Appl. Energy Mater. 1, 725–735 (2018).

58. Aegerter, M. A. & Mennig, M. Sol-Gel Technologies for Glass Producers and Users. (Kluwer Academic Publishers, 2004).

59. Kistler, S. F. & Schweizer, P. M. Liquid Film Coating: scientific principles and their technological implications. (Springer-Science and Business Media, 2012).

60. Chilvery, A., Das, S., Guggilla, P., Brantley, C. & Sunda-Meya, A. A perspective on the recent progress in solution-processed methods for highly efficient perovskite solar cells. Science and Technology of Advanced Materials 17, 650–658 (2016).

61. Maleki, M., Reyssat, M., Restagno, F., Quéré, D. & Clanet, C. Landau–Levich menisci. Journal of Colloid and Interface Science 354, 359–363 (2011).

62. Wilson, S. D. R. The drag-out problem in film coating theory. J Eng Math 16, 209–221 (1982).

63. Xu, D. & Neckers, D. C. Aggregation of rose bengal molecules in solution. Journal of Photochemistry and Photobiology A: Chemistry 40, 361–370 (1987).

64. Deng, Y. et al. Surfactant-controlled ink drying enables high-speed deposition of perovskite films for efficient photovoltaic modules. Nat Energy 3, 560–566 (2018).

65. Ernst, M., Herterich, J.-P., Margenfeld, C., Kohlstädt, M. & Würfel, U. Multilayer Blade-Coating Fabrication of Methylammonium-Free Perovskite Photovoltaic Modules with 66 cm 2 Active Area. Solar RRL 6, 2100535 (2022).

66. Le Berre, M., Chen, Y. & Baigl, D. From Convective Assembly to Landau−Levich Deposition of Multilayered Phospholipid Films of Controlled Thickness. Langmuir 25, 2554–2557 (2009).

67. Ruschak, K. J. Coating Flows. Annu. Rev. Fluid Mech. 17, 65–89 (1985).

68. Stafford, C. M., Roskov, K. E., Epps, T. H. & Fasolka, M. J. Generating thickness gradients of thin polymer films via flow coating. Review of Scientific Instruments 77, 023908 (2006).

69. Cebe, S. The Effect of Viscosity in Beveled Blade Coating. (Western Michigan Wuniversity, 1993).

70. Sullivan, T. M. & Middleman, S. Film thickness in blade coating of viscous and viscoelastic liquids. Journal of Non-Newtonian Fluid Mechanics 21, 13–38 (1986).

71. Martínez, S. R. et al. Self-Sterilizing 3D-Printed Polylactic Acid Surfaces Coated with a BODIPY Photosensitizer. ACS Appl. Mater. Interfaces 13, 11597–11608 (2021).

72. Nalsby, AndrewJ. INKJET RECORDING SHEET COMPRISING A CHROMOPHORE-GRAFTED POLY WINYL ALCOHOL. 7 (2001).

73. Ichimura, K., Iwata, S., Mochizuki, S., Ohmi, M. & Adachi, D. Revisit to the photocrosslinking behavior of PVA-SbQ as a water-soluble photopolymer with anomalously low contents of quaterized stilbazol side chains. J. Polym. Sci. A Polym. Chem. 50, 4094–4102 (2012).

74. Fila, G. et al. Murine Model Imitating Chronic Wound Infections for Evaluation of Antimicrobial Photodynamic Therapy Efficacy. Front. Microbiol. 7, (2016).

75. Garcia-Sampedro, A., Tabero, A., Mahamed, I. & Acedo, P. Multimodal use of the porphyrin TMPyP: From cancer therapy to antimicrobial applications. J. Porphyrins Phthalocyanines 23, 11–27 (2019).

76. Lamberts, J. J. M., Schumacher, D. R. & Neckers, D. C. Novel rose bengal derivatives: synthesis and quantum yield studies. J. Am. Chem. Soc. 106, 5879–5883 (1984).

77. Dancer, S. J. Importance of the environment in meticillin-resistant Staphylococcus aureus acquisition: the case for hospital cleaning. The Lancet Infectious Diseases 8, 101–113 (2008).

78. Joshi, R. & Taylor, E. Contact Transmission, Part 2: Materials, Design, and Cleaning. 23 https://www.healthdesign.org/insights-solutions/contact-transmission-part-2-materials-design-and-cleaning (2019).

79. Ebata, Y., Croll, A. B. & Crosby, A. J. Wrinkling and strain localizations in polymer thin films. Soft Matter 8, 9086 (2012).

80. Singh, N., Verma, A., Sachan, P., Sharma, A. & Kulkarni, M. M. Self-Organized Wrinkling in Thin Polymer Films under Solvent–Nonsolvent Solutions: Patterning Strategy for Microfluidic Applications. ACS Appl. Polym. Mater. 3, 6198–6206 (2021).

81. Das, A., Banerji, A. & Mukherjee, R. Programming Feature Size in the Thermal Wrinkling of Metal Polymer Bilayer by Modulating Substrate Viscoelasticity. ACS Appl. Mater. Interfaces 9, 23255–23262 (2017).

82. Ding, F. & Giacomin, A. J. Die Lines in Plastics Extrusion. Journal of Polymer Engineering 20, (2000).

83. Khurana, R. et al. Supramolecular Nanorods of (N-Methylpyridyl) Porphyrin With Captisol: Effective Photosensitizer for Anti-bacterial and Anti-tumor Activities. Front. Chem. 7, 452 (2019).

84. Baranovskii, S. F., Bolotin, P. A. & Evstigneev, M. P. Aggregation of 1,3,7-trimethylxanthine with methylene blue in aqueous solution. J Appl Spectrosc 73, 171–177 (2006).

85. Fernández-Pérez, A. & Marbán, G. Visible Light Spectroscopic Analysis of Methylene Blue in Water; What Comes after Dimer? ACS Omega 5, 29801–29815 (2020).

86. Milošević, M. D., Logar, M. M., Poharc-Logar, A. V. & Jakšić, N. L. Orientation and Optical Polarized Spectra (380–900 nm) of Methylene Blue Crystals on a Glass Surface. International Journal of Spectroscopy 2013, 1–6 (2013).

87. Mahmood, T., Anwer, F., Mahmood, I., Kishwar, F. & Wahab, A. Solvatochromic effect of Methylene Blue in different solvents with different polarity. European Research Journal 1, 1202–1215 (2013).

88. Heyne, B. et al. Investigation of singlet oxygen reactivity towards propofol. Photochem. Photobiol. Sci. 2, 939 (2003).

89. Mendes, B. et al. Influence of Rose Bengal Dimerization on Photosensitization. Photochem Photobiol 97, 718–726 (2021).

90. Dimitriev, O. P., Piryatinski, Y. P. & Pud, A. A. Evidence of the Controlled Interaction between PEDOT and PSS in the PEDOT:PSS Complex via Concentration Changes of the Complex Solution. J. Phys. Chem. B 115, 1357–1362 (2011).

91. Håkansson, A. et al. Effect of (3-glycidyloxypropyl)trimethoxysilane (GOPS) on the electrical properties of PEDOT:PSS films. J. Polym. Sci. Part B: Polym. Phys. 55, 814–820 (2017).

92. Lee, J. et al. Formation of a conductive overcoating layer based on hybrid composites to improve the stability of flexible transparent conductive films. RSC Adv. 9, 4428–4434 (2019).

93. Koyama, K., Okada, M. & Nishimura, M. An interpolymer anionic composite reverse osmosis membrane derived from poly(vinyl alcohol) and poly(styrene sulfonic acid). J. Appl. Polym. Sci. 27, 2783–2789 (1982).

94. Michele, A. et al. Acid catalyzed cross-linking of polyvinyl alcohol for humidifier membranes. J Appl Polym Sci 139, 51606 (2022).

95. Nishimura M., Yabu M. & Sugihara M. Ion Exchange Membranes. X. Cation-Selective Membranes Prepared from Polystyrenesulfonic Acid and Polyvinyl Alcohol. The Journal of the Society of Chemical Industry, Japan 70, 393–398 (1967).

96. Brody, H. Overdyeing and Diffusion of Acid Dyes in Nylon. Textile Research Journal 35, 844–850 (1965).

97. Farouk, R. & Gaffer, H. E. Simultaneous dyeing and antibacterial finishing for cotton cellulose using a new reactive dye. Carbohydrate Polymers 97, 138–142 (2013).

98. Soleimani-Gorgani, A. & Taylor, J. A. Dyeing of nylon with reactive dyes. Part 3: Cationic reactive dyes for nylon. Dyes and Pigments 76, 610–623 (2008).